SUPPORTING INFORMATION

Structural Dynamics of Lateral and Diagonal Loops of Human Telomeric G-quadruplexes in Extended MD Simulations

Barira Islam,[1] Petr Stadlbauer,[1] Miroslav Krepl,[1] Marek Havrila,[1] Shozeb Haider[2] and Jiri Sponer[1]*

[1] Institute of Biophysics of the Czech Academy of Sciences, Královopolská 135, 612 65 Brno, Czech Republic

[2] UCL School of Pharmacy, 29-39 Brunswick Square, London WC1N 1AX, UK

[*] To whom correspondence should be addressed. Tel: 420 541 517 133; Fax: +420 541 212 179; Email: sponer@ncbr.muni.cz

SUPPORTING METHODS

Equilibration protocol: For equilibration, the system was first minimized with 500 steps of steepest descent followed by 500 steps of conjugate gradient minimization with 25 kcal mol^{-1} A^{-2} position restraints on DNA atoms. It was then heated from 0 to 300 K for 100 ps with constant volume and position restraints of 25 kcal mol^{-1} A^{-2}. Minimization with 5 kcal mol^{-1} A^{-2} restraints followed, using 500 steps of steepest descent method and 500 steps of conjugate gradient. The restraints of 5 kcal mol^{-1} A^{-2} were maintained on DNA atoms and the system was equilibrated for 50 ps at constant temperature of 300 K and pressure of 1 atm. An analogous series of alternating minimizations and equilibrations followed using decreasing position restraints of 4, 3, 2 and 1 kcal mol^{-1} A^{-2} consecutively. The final equilibration was carried out with position restraints of 0.5 kcal mol^{-1} A^{-2} and starting velocities from the previous equilibration, followed by a short free molecular dynamics simulation of 50 ps. Temperature and pressure coupling during equilibration was set to 0.2 and coupling during the last molecular dynamics phase was set to 5.

Method for the comparison of experimental NMR structure with the simulation ensembles: The simulation trajectories were analysed in ptraj and cpptraj modules of Amber14 and the program xmgrace was used to prepare the graphs.

The agreement of simulations with the respective primary experimental data was assessed by computing distance violations of experimental intermolecular NOE (Nuclear Overhauser Effect) distances. For this, supertrajectories of simulation ensembles were made by joining the trajectories of all simulations (irrespective of the force field, water model and ionic conditions) belonging to one PDB structure. The weighted average of the NOE distances in the simulation ensemble in the supertrajectory was computed for the lateral, diagonal loops and flanking bases. It was calculated as $(\frac{1}{n}\sum_{i=1}^{n} r^{-6})^{(-1/6)}$, where r_i is instantaneous distance between the two atoms in *i*-th supertrajectory frame and *n* is the total number of frames in the supertrajectory. This value was then compared with the experimental upper-bound values of the NOE data. Only the proton pairs of inter-residue base pairs related to flanking bases and LLs and with experimental upper-bound NOE data of < 6 Å were considered. NOEs related to PLs were investigated if they formed any alignments with LLs. The NMR restraints data of only PDB structures 2KF8, 2MBJ, 2GKU and 2JSM are available on the PDB server so a comparison of NOE distances in the experiments and simulation ensembles of these structures could be carried out.

SUPPORTING RESULTS

Survey of ambiguities in experimental NMR structures

As noted in the main text, experimental evaluation of GQ loop conformations is not always straightforward. The loop regions are often underdetermined by the primary NMR data and in addition the NMR data typically reflect ensemble-averaged properties, which complicate the use of the data directly as restraints in the simulations. Such restraints can distort the simulations when multiple co-existing substates are sampled by the real molecules and contribute to the measured data. Therefore, especially when the loops are in reality flexible, the refined NMR structures may be affected by some uncertainties and influenced by the refinement protocol. In

the Htel NMR structures, loop bases in some of the PDB files show variable arrangements in the deposited models. In some cases, variations in the NMR models may not reflect real dynamics of the molecules but rather insufficient capability of the primary data to determine the structure which is then influenced by the refinement protocol. Indeed, in some cases we have noticed occasional inconsistencies in the structure descriptions as presented in the original papers and the actual structures deposited in the database. Therefore, we surveyed the PDB structures, contrasted them with the NOE data, with discussion based on the primary data as presented in the corresponding papers and compared them with the MD simulations. The summary of the found differences is presented below and gives some insights into the potential uncertainties in the experimental structures.

143D

The A1:A13 base pair.

According to the original publication, sequential NOEs were detected between A1 and G2 and A13 and G22 in the NMR experiment that defined the structure of 143D. This can be attributed to A1 and A13 stack on G2 and G22, respectively. There is no discussion in the paper regarding the A1:A13 base pairing.

PDB: There is A1:A13 *cis* Hoogsteen-Hoogsteen base pair in half of the models and in other half A1 and A13 do not interact and just stack on G2 and G22, respectively. It indicates the base pairing cannot be inferred from the NMR data and may be a consequence of the refinement protocol. A1 and A13 stack on G2 and G22 is present in all the models of the PDB structure.

MD simulations: We carried out five different simulations of 143D and A1:A13 Hoogsteen/Hoogsteen base pairing was sampled in only one of them, namely, the OL15 simulation with K^+ and TIP3P. In the bsc0χ_{OL4} simulations, A1 and A13 formed Watson-Crick (WC)/Hoogsteen base pair while in the other simulations Hoogsteen and sugar edge faces were used to form the hydrogen bonds.

T18|A19 stack

According to the original publication, T17 and T18 are poorly defined in the experiment. Sequential NOEs from -CH_3 of T17 to G16 and a long range NOE to the H8 of G15 were detected in the original experiment. Sequential NOEs were also detected at the T17|T18 and T18|A19 steps in the LL2.

PDB: In the first three models, T17 is exposed to the solvent while T18 is stacked below the A19|G-stem. In the models 4, 5 and 6, both T17 and T18 are exposed to the solvent. It confirms that the stacking of T18 below the A19|G-stem cannot be inferred from the NMR data.

MD simulations: In all the MD simulations with the first model of PDB as the starting structure, T17 remained exposed to the solvent while T18 stacked below the A19|G-stem throughout the simulation. We also carried out five simulations with model 4 as the starting structure. In this model, both T17 and T18 are exposed to the solvent. In four simulations, LL2 attained model 1 like conformation (type-1) as T18 moved to stack below the A19|G-stem, while T17 remained exposed to the solvent. Further details of these simulations are given below in separate section.

2KF8

T5:T17 base pair.

According to the original publication, there is a possibility of T5:T17 base pair at the bottom of the G-stem. The primary NMR data associated with the structure does not show NOEs associated with T5 and T17 base pair.

PDB: In all the structures, T17 stacks below T5 and the T5:T17 base pair is not present in any of the models.

MD Simulations: T5:T17 base pair was mostly stable in two out of three simulations. In one simulation, T5:T17 was sampled for ~28% of the simulation time.

2MBJ

A15:A9:T25 triplet.

According to the original publication, A9:T25 WC base pair is present below the G-stem. A15 from the PL also stacks below the G-stem, potentially establishing interactions with this base pair. The primary NMR data suggests an NOE distance of 3.6 to 6.0 Å between A9(H2) and A15(H2).

PDB: A9:T25 base pair was present in all the models while A15 does not interact with either A9 or T25 in any of the models.

MD simulations: A9:T25 (WC) interaction was sampled in all the simulations but only one of the simulations (bsc0χ_{OL4}) sampled A15 interaction with this base pair. A9:T25 interaction was intermittent in bsc0$\chi_{OL4}\varepsilon\zeta_{OL1}$ simulation.

A21 interaction with A3:T20

According to the original publication, A3 and T20 form a WC base pair and A21 interaction with the base pair can form a triple platform above the first quartet. The primary NMR data suggests NOE distances of 4.5 to 7.5 Å between A21(H2) and A3(H1'), 2.85 and 4.75 Å between A3(H2) and A21(H2) and 3.6 to 6.0 Å between A3(H2) and A21(H8).

PDB: In the PDB structures, A3 and T20 are not coplanar in any of the models and in some of the models, the presumably interacting heteroatoms are >3.5 Å apart. A21 also is not coplanar with these bases in any of the models. So, the triple noticed in the text is not seen in the PDB structures.

MD simulations: A3:T20 WC base pair was stable in four out of five simulations, giving strong MD support for the existence of this base pair. A21 could align with this base pair only in bsc0χ_{OL4} simulation and so the triple was sampled in only one simulation.

2HY9

A3:A9:A21 triple.

According to the original publication, A3, A9 and A21 triple is present on the top of the G-stem. Strong NOE was detected between A3(H2) and A21(H2) and weak NOE was observed between A9(H1') and A3(H2).

PDB: In the PDB structure, A9 is not coplanar with A3 and A21 and does not form hydrogen bond with these bases.

MD simulations: A3:A21 interaction was sampled in all of the simulations, consistent with the strong NOE signals between A3 and A21. None of the simulations sampled A9 interaction with A3 and A21 and the triple is not supported by the simulations.

2JPZ

A9:T8:T25 triple.

According to the original publication, A9:T8:T25 triple is present below the G-stem. Clear NOEs were detected between T8(H1') and A9(H8) and T8(H3) and T25(H1') in the NMR experiment.

PDB: In the PDB structures, T8 and T25 form two hydrogen bonds while A9 forms just one hydrogen bond with T25.

MD simulations: The triple was sampled in two out of the three simulations, giving quite strong support for the existence of the triple.

Description of the individual simulation trajectories

For list of base pairs in starting structures and all simulations see the Table 3 in the main text.

143D

In the starting structure of 143D simulations (model 1), the first thymines of both the LLs, T5 and T17 are exposed to the solvent and do not form any major structural alignment. T6 and A19

stack below the third quartet and form a T6:A19 pair by WC bonding (Figure 6a). A7 is aligned in the groove while T18 is stacked below the A19.

143D in 10 μs bsc0χ_{OL4} simulation: In the simulation, T5 and T17 remained exposed to the solvent. T6:A19 WC base pair was stable (Figure S17a) and A7 could not stack below the G-stem during the course of the simulation. T18|A19|G-stem stack was also stable in the simulation.

The terminal base A1 and A13 from the DL are stacked over G2 and G22 respectively in the starting structure. Within the initial 100 ns, A1 moved from its position to stack with G14 and formed *trans* WC-Hoogsteen base pair with A13 which was stable for ~4.2 μs (Figure S12a). The thymine bases of the DL, T12 and T11 stacked over on A1 meantime. The DL was more dynamic in the later 5.8 μs of the simulation. This was initiated by the change in orientation of A1 from *anti* to *syn* position after ~4.2 μs. A1 moved towards the groove and could not stack further with the terminal quartet and the base pairing between A1 and A13 was disrupted. Following this, A13 (*syn*) which was originally stacking on G22 (*syn*) moved from its position to stack over G14 (*anti*). T12 and T11 stacked over A13 and the DL formed an untwisted ladder resembling structure by the partial stacking of the bases. This structure lasted until the end of the simulation (Figure S15a).

143D in 10 μs bsc0$\chi_{OL4}\varepsilon\zeta_{OL1}$ simulation: The first thymines of the LLs remained exposed to the solvent as in the starting structure. T6:A19 base pair was stable throughout the simulation (Figure S17b). A7 was exposed to the solvent and aligned at an angle to the G-stem. The LL2 also maintained its original arrangement as T17 was exposed to the solvent and T18 and A19 stacked below the G-stem throughout the simulation.

The stacking interactions in the DL were evident but interconversion of conformations along the course of trajectory was observed. The terminal A1:A13 base pairing as in bsc0χ_{OL4} force field was not sampled in bsc0$\chi_{OL4}\varepsilon\zeta_{OL1}$ simulation. In the first 1.3 μs of the simulation, A1 and A13 continued to stack on G2 and G22 without any hydrogen bond interaction between A1 and A13.

T11 was exposed to the solvent and T12 sampled two conformations. In one conformation, T12 stacked on A1 and in the other conformation, T12 and T11 both stacked together and were exposed to the solvent. At 1.3 μs, T11 and T12 moved to stack with A1 and then A1|T12|T11 stack aligned perpendicularly over G-stem was stable until 2.2 μs. A1 then moved to stack again over G2. Following this, A13 aligned at an angle with T11 and T12 and did not stack on the G-stem bases (Figure S13). This arrangement of the loop lasted until the end of the simulation.

143D in 5 μs OL15 simulation: The LLs in the OL15 simulation behaved similarly as in the bsc0χ_{OL4} and bsc0$\chi_{OL4}\varepsilon\zeta_{OL1}$ simulations. In the LL1, T5 was exposed to the solvent and hydrogen bond between T5(O4) and G9(H22) stabilized its position. The T6:A19 interaction was stable below the third quartet (Figure S17c). A7 was also exposed to the solvent and its position was stabilized by A7(H4')-G8(N3) interaction. In the LL2, T17 was also exposed to the solvent and stabilized by a hydrogen bond interaction between T17(O4) and G16(H22). T18 stacked below A19 and was stable throughout the simulation.

T11 and T12 stacked together and could occupy three different positions. The stack could be either stacked on A1 or A13 or aligned vertically along the loop to be exposed to the solvent. The terminal bases A1 and A13 of the DL stacked on G2 and G22 as in the starting structure but did not form any A1:A13 interactions initially. At ~1.3 μs, A13 aligned perpendicularly to G22 and formed A13(H8) -G22(N3) hydrogen bond. A13 then moved to interact with T11|T12 stack and its amino group formed hydrogen bond interaction with T11(O2) and T12(O2). A13 again stacked with G22 and A1 moved between G2 and G14 and formed A1(H61)-A13(N3) and A1(N1)-A13(H2) hydrogen bonds between 2.6 to 4.6 μs (Figure S12b). In the last 400 ns of the simulations A1 aligned along the groove while T11 and T12 stacked over A13 to form a ladder-like structure as in the bsc0χ_{OL4} simulation.

143D in 5 μs SPC/E OL15 simulation with K^+ as the stabilizing ion: In the LLs, T6:A19 base pair was stable throughout the simulation (Figure S17d). The position of T5 in the groove was stabilized by T5(O4)-G9(H22) hydrogen bond which was maintained throughout the simulation.

A7 was aligned in the groove and was stabilized with either A7(H61)-T18(O2) or A7(H62)-G20(O4') hydrogen bonds. The T17(O4)-G16(H22) interaction was not always maintained as sometimes T17 moved towards the solvent farther from G16 and then again formed the hydrogen bond. T18 was stacked below A19 during the entire simulation.

In the DL, T11 and T12 stack together and then stacked on A13 early in the simulation to form T11|T12|A13 ladder. A1 moved to align over somewhere between G2 and G14 at ~1 μs and finally formed *cis* WC/sugar edge hydrogen bonds with A13 (Figure S12c). This arrangement was stable throughout the simulation.

143D in 5 μs TIP3P OL15 simulation with K^+ as the stabilizing ion: In the LL1, T5 aligned in the groove and formed T5(O4)-G3(H8) hydrogen bond. This bond was intermittent as T5 moved towards the solvent in 30% of the frames of the simulation. A7 was also aligned in the groove and formed a stable A7(H61)-T18(O2) hydrogen bond. In the LL2, the position of T17 in the groove was stabilized by T17(O4)-G16(H22) interaction. The position of T18 and A19 was maintained as in the starting structure, i.e., it was stacked below the G-stem.

On top of the G-stem, A1 stacked on G2 and A13 moved between G14 and G22. A1 and A13 formed *cis* Hoogsteen-Hoogsteen base pair similar to the starting structure and it was sampled in 70% of the frames of the simulation (Figure S12d). T11 and T12 stacked together and stacked on A13 and this ladder resembling structure was stable throughout the simulation.

143D model 4 in five 3-5 μs OL15 simulations: Models 4, 5 and 6 of 143D differ from models 1, 2 and 3 in the conformation of LL2. The LL2 is in type-1 conformation in models 1, 2 and 3 but in models 4, 5 and 6, T18 of LL2 is also exposed to the solvent along with the T17 and only A19 is stacked below the G-stem and forms T6:A19 base pair (Figure S10a). We carried out five independent 3-5 μs simulations of 143D model 4 to study the LL2 dynamics.

In three simulations, LL2 attained type-1 conformation within 200 ns as T18 moved to stack below A19 and T17 remained exposed to the solvent (Figure S10b, c and d). In the fourth simulation, T18 moved to stack below A19 at ~2.3 μs and the LL2 thus attained the type-1

conformation (Figure S10e). In the fifth simulation T6:A19 WC base pair was not sampled as at ~150 ns A19 moved towards the solvent. In the LL2, T18 and A19 were stacked together and exposed to the solvent (Figure S10f). T17 was also exposed to the solvent but occupied multiple positions with respect to T18|A19 without forming any stable interaction.

The conformation of LL1 as in the starting conformation was maintained in all the simulations for most of the time as T5 and A7 were exposed to the solvent and T6 was stacked below G-stem. In the DL, T11|T12|A13 was sampled throughout the simulations. Thus, in contrast to the dynamics of LL2, LL1 and DL dynamics was similar to the simulations based on model 1.

2KF8

The two-quartet GQ of Htel sequence $GGG(TTAGGG)_3T$ is a case of two-quartet fold due to slipped first strand (Figure 1b). It comprises LL1 formed by GTTA, DL formed by GTTAG and LL2 formed by TTA sequence. The G3 and A6 of LL1 participate in forming a triad with A18 of LL2 below the G-stem. G3 interacts with both A6 and A18 but there are no direct hydrogen bonds between A6 and A18. In the DL, residues G13:G9:G21 form a triad alignment over the first quartet.

2KF8 in 10 µs bsc0χ_{OL4} simulation: The native interactions of LL were maintained throughout the simulation. T4 of LL1 was aligned in the groove while T5 formed base pair with T17 of the LL2 (Figure S26a) below the A6:G3:A18 triple within 5ns of the simulation. In the LL2, T16 was aligned in the groove of the G-stem. T17 was stacked below G-stem while A18 formed a triple with bases of LL1.

In the starting structure, G9 forms Hoogsteen base pair with G21 while both G9 and G21 form one single hydrogen bond with G13. This alignment was stable until the end of the simulation. T10 of DL was exposed to the solvent. T11 maintained stable base pair with 3'-flanking base T22 (Figure S25a), while A12 stacked on T11 during the entire simulation time.

2KF8 in 10 μs bsc0$\chi_{OL4}\varepsilon\zeta_{OL1}$ simulation: The G3:A6:A18 and G13:G9:G21 triples were maintained throughout the simulation as in the bsc0χ_{OL4} simulation.

In the LL1, T4 was exposed to the solvent and T5:T17 base pair below the G3:A6:A18 triple was maintained until 2.8 μs. At 2.8 μs, T4 moved to stack below G3 and formed base pair with T17 (Figure S26b) while T5 moved to stack below T4. T16 of LL2 was exposed to the solvent and was more flexible in this simulation. The T11 and T22 interaction was not very stable in this simulation and fluctuating H-bonds were formed (Figure S25b). A12 stacked above T11 during the simulation.

2KF8 in 5 μs OL15 simulation: The G3:A6:A18 and G13:G9:G21 triples were maintained throughout the simulation as in the other two simulations. In the LL1, T4 was exposed to the solvent while the T5 and A6 stacked below the G-stem participating in base pair and base triple, respectively. The T5:T17 base pair below the base triple was intermittent (Figure S26c) but mostly stable in the simulation. In the LL2, T16 was aligned in the groove forming a stable G15(H22)-T16(O4) bond. T17 and A18 were stabilized by interaction with T5 and base triple below the G-stem, respectively.

In the DL, T10 was exposed to the solvent while T11 formed a base pair with 3'-flanking base T22 on top of the G13:G9:G21 triple. T11:T22 interaction was intermittent (Figure S25c) but T11 and T22 stacked on G-stem throughout the simulation.

2MBJ

The 27-mer (2+2) antiparallel GQ has TTA nucleotides at the 5'- and 3'-ends. These nucleotides can arrange to form capping structure both over and below the G-stem. Among the 5'-flanking bases, A3 is stacked over the first quartet while T1 and T2 are present over it but do not form any stable interaction. In the LL1, T7 is exposed to the solvent while T8 and A9 stack below G-stem. In the LL2, T19 is exposed to the solvent, T20 stacks below G-stem and forms WC base pair with A3 and A21 is aligned at an angle to the G-stem.

2MBJ in 10 μs bsc0χ_{OL4} simulation: In the bsc0χ_{OL4} simulation, T1 stacked over T2 and A3 such that all the three nucleotides stacked over each other sequentially.

The structure of LL1 was maintained in the simulation. In the starting structure, A9 of the LL1 forms a base triple below the G-stem with flanking base T25 and A15 of the PL. The A15:A9:T25 triple was stable throughout the bsc0χ_{OL4} simulation (Figure S19a). Also, T8 formed a stable base pair with A27 during the simulation (Figure S19b).

T19 was flexible during the simulation but remained exposed to the solvent. T20:A3 WC base pairing as in the starting structure was stable throughout the simulation (Figure S18a). A21 also moved to be in plane with this base pair and a true A3:T20:A21 triple was sampled from 1.35 to 10 μs. The flanking bases T25, T26 and A27 stacked below the G-stem. T25 participated in the formation of base triple and T26 stacked below A27 which formed WC base pair with T8 of LL1.

2MBJ in 10 μs bsc0$\chi_{OL4}\varepsilon\zeta_{OL1}$ simulation: The T1|T2|A3 stack was sampled in this simulation as well. In the LL1, T7 was exposed to the solvent and did not form any stable interaction in the simulation. T8:A27 base pair was not observed in this simulation. Instead, T8 stacked below A9 that stacked below G6. The native A9:T25 base pair was intermittent and A15 interaction with T25 was also not sampled in the bsc0$\chi_{OL4}\varepsilon\zeta_{OL1}$ simulation (Figure S19c). In the LL2, T19 aligned in the groove and formed T19(O4)-G17(H22) interaction with guanine of the second quartet. The interaction between T20 and A3 was stable throughout the simulation (Figure S18b) but in this simulation A21 did not align with the base pair and thus the respective triple could not be formed. A21 aligned in the groove. Among the 3'-flanking bases, T25 formed intermittent interactions with A9 and T26 stacked below T25 but did not form any stable hydrogen bond. A27 stacked below G16 throughout the simulation.

2MBJ in 5 μs OL15 simulation: T1|T2|A3 stacked over the G-stem and A3:T20 base pair was stable in this simulation as well (Figure S18c). A21 was aligned in the groove and hence A3:T20:A21 triple above the G-stem was not sampled. In the LL1, T7 was exposed to solvent

and its position was stabilized by T7(O4)-G6(H22) interaction. T8 and A9 stacked below the G-stem throughout the simulation. A9 was aligned between T25 and T26 and sampled bifurcated H-bonds A9(H62)-T25(O4) and A9(H62)-T26(O2). In the second lateral loop, T19 moved over the G-stem and formed base pair with T1 for 50% of the simulation time. As mentioned earlier, position of T20 was stabilized by interaction with A3 and A21 was aligned in the groove in this simulation. Among the three 3'-flanking bases, T25 and T26 stacked below G24 of the third quartet and interacted with A9 while A27 stacked below A15. Thus the base triples both above and below the G-stem were not maintained in the simulation.

2MBJ in 5 μs SPC/E OL15 simulation with K^+ as the stabilizing ion: In this simulation, T1|T2 stack did not align on A3 and was exposed to the solvent while A3:T20 base pair was stable (Figure S18d). In the LL1, T7 was exposed to the solvent while T8 formed base pair with flanking base T26. A9 formed base pair with flanking base T25 (Figure S19e). The A9:T25 was stable throughout the simulation and again A15 interaction with T25 was not sampled. A27 moved in plane with A9:T25 base pair to form stable A9:T25:A27 triple (Figure S19e). However, there was no direct interaction between A9 and A27. The T8:T26 base pair was intermittent in the simulation. In frames when T8:T26 base pair was not formed, T8 either stacked with T7 or was stacked below T26. In LL2, T19 was exposed to the solvent while the T20 stacked on the G-stem and formed A3:T20 base pair (Figure S18d). A21 aligned in the groove and could not form any stable interaction. The native triples were not sampled in this simulation as well. The position of 3'-flanking bases T25, T26 and A27 was stabilized by interaction with LL1 bases.

2MBJ in 5 μs TIP3P OL15 simulation with K^+ as the stabilizing ion: The T1|T2 stack was exposed to the solvent and could not align over A3. The A3:T20 base pair was stable throughout the simulation (Figure S18e) and A21 was aligned in the groove, therefore the triple above the G-stem was not sampled. In the LL1, T7 was exposed to the solvent while T8 either stacked below T26 or formed T8:T26 base pair intermittently. A9 stacked below G-stem and A9:T25 base pair was stable in this simulation and again A15 did not interact with T25 (Figure S19f). In

the LL2, T19 was exposed to the solvent, T20 formed stable base pair with A3 and A21 aligned in the groove throughout the simulation. The position of 3'-flanking bases, T25, T26 and A27 was stabilized by the interactions with loop bases.

2HY9

In 2HY9, the three adenines, flanking base A3, A9 from the PL and A21 from LL2 stack on the G-stem. In the starting structure, A3 and A21 form *cis* WC base pair but A9 is not coplanar and does not form hydrogen bond with these bases.

2HY9 in 10 µs bsc0χ_{OL4} simulation: In this simulation, A9 of the PL moved from the top of the GQ in the equilibration stage as soon as the restraints were lifted and stacked with T8 in the groove. A3 and A21 continued to stack on G4 and G22, respectively and sampled *cis* Hoogsteen-WC interactions, however, in many simulation frames A3 and A21 were staggered (Figure S20a). The flanking bases A1 and A2 stacked on A3. A2 formed base pair with T20 of LL2 (Figure S21a). In the LL1, T13 was exposed to the solvent while T14 interacted with flanking A25. T14:A25 interaction was maintained in the simulation (Supporting Figure S21c). A15 of the LL1 was exposed towards the solvent. In the LL2, T19 was exposed to the solvent and was stabilized by T19(O2)-A21(H62) bond. T20 and A21 stacked on G-stem and interacted with the A2 and A3, respectively. The 3'-flanking base A25 interacted with T14 of LL1 while A26 was either exposed to the solvent or stacked below A25.

2HY9 in 10 µs long bsc0$\chi_{OL4}\varepsilon\zeta_{OL1}$ simulation: In the bsc0$\chi_{OL4}\varepsilon\zeta_{OL1}$ simulation, A9 moved from top of the GQ within 5 ns of the simulation. The A3 and A21 continued to stack on G4 and G22 respectively and maintained the hydrogen-bond interaction between them although they were staggered in many frames similar to the bsc0χ_{OL4} simulation (Figure S20b). A2 and A1 stacked on A3. T13 of LL1 was aligned in the groove and sampled T13(O4)-G18(H22) hydrogen bond interaction in 60% of the frames. T14 aligned below the G-stem and its interaction with A25 was stable throughout the simulation (Figure S21d). A15 of LL1 was exposed to the solvent in this simulation as well. In the LL2, T19 and T20 stacked together and were exposed to the

solvent so that the A2:T20 base pair could not be sampled. A21 stacked over G22 and formed base pair with A3.

2HY9 in 5 μs OL15 simulation: The three 5'-flanking adenines of the structure aligned sequentially over the G-stem. The position of A2 was stabilized by the interaction with T20 of the LL2 which was stable throughout the simulation (Figure S21b). Early in the simulation, A9 again moved from the top of the G-stem and the A3:A21 pair was sampled in the simulation (Figure S20c). In the LL1, T13 was exposed to the solvent for all of the simulation time. T14 sampled base pair with A25 for 2 μs and then A25 moved to solvent. A15 moved to stack below G24. In the LL2, T19 was exposed to the solvent and the T20 and A21 were stacked on the G-stem. The 3'-flanking bases A25 and A26 stacked below the G-stem but the stack was flexible and was sometime exposed to the solvent.

2GKU

In the starting structure, the flanking base T1 forms WC base pair with A20. T2 aligns over T1 and forms a hydrogen bond with T19. In the LL1, T12 is exposed to the solvent while T13 forms hydrogen bond interaction with flanking base A24. A14 of LL1 is also exposed to the solvent. In LL2, T18 is exposed to the solvent, while T19 and A20 stack over G-stem. Both T19 and A20 form hydrogen bonds with the flanking nucleotides. The 3'-flanking nucleotide A24 interacts with T13.

2GKU in 10 μs bsc0$\chi_{OL4}\varepsilon\zeta_{OL1}$ simulation: In the simulation, T1:A20 base pair was stable throughout the simulation (Figure S22a). Interaction of T2 with T19 was not stable as T2 occasionally flipped towards the solvent (Figure S28a). In the LL1, the interaction between T13 and A24 was not stable as at ~440 ns T12 moved to interact with A24 (Figure S22b) while T13 moved to stack below T12. A14 of LL1 also sampled hydrogen bonds with T12 and A24 of T12:A24 base pair. In LL2, T18 was oriented in the groove and its position was stabilized by hydrogen bond interaction T18(O4)-G17(H22). This interaction was stable throughout the simulation except a few instances between 1-2 μs and 5.5-6.5 μs. T19 and A20 stacked over the

G-stem and were stable throughout the simulation. The 3'-flanking base A24 was stacked below the G-stem and interacted with LL1.

2GKU in 5 μs SPC/E OL15 simulation with K^+ as the stabilizing ion: T1:A20 base pair was stable in the simulation (Figure S22c). T2 and T19 hydrogen bond as in the starting structure was sampled (Figure S28b). In LL1, T12 was exposed to the solvent while T13 was stacked below G11 of the third quartet and formed base pair with A24. A14 oriented towards the G-stem and stacked below A24|G23. At ~2.3 μs T12 moved to stack below G11 and T13 moved to stack below the T12. T12 formed base pair with A24 (Figure S22d). In LL2, T18 was exposed to the solvent while T19 and A20 stacked on the first quartet. The position of T19 and A20 was stabilized by interaction with flanking bases. The 3'-flanking base A24 stacked below G23 of the third quartet.

2GKU in 5 μs TIP3P OL15 simulation with K^+ as the stabilizing ion: The residues T1 and T2 maintained their interactions with A20 and T19, respectively (Figure S22e, S28c). In LL1, T12 was exposed to the solvent, T13 stacked below G11 and maintained base pair with A24 (as in the starting structure) throughout the simulation (Figure S22f). A14 stacked with A24|G23. In LL2, T18 was exposed to the solvent, while T19 and A20 stacked on the G-stem.

2JSM

In the starting structure, T1, A2 and A20 form a triple on the G-stem.

2JSM in 10 μs bsc0$\chi_{OL4}\varepsilon\zeta_{OL1}$ simulation: Early in the simulation, A2 moved over T1 and A20. A2 then formed a stable *trans* WC base pair with T19 of LL2. T1:A20 WC base pair was stable for most of the simulation time (Figure S23a). In LL1, T12:A14 sampled native Hoogsteen interaction until 3.6 μs and then *trans* WC pairing was sampled from 4.5 μs until the end of the simulation (Figure S23b). T13 stacked below T12 for all the simulation time. In the LL2, T18 was exposed to the solvent and its position was stabilized by T18(O2)-A20(H62) hydrogen bond which was stable for most of the simulation time. T19 and A20 stacked on the G-stem and

their positions were stabilized by hydrogen bond interactions with the 5'-flanking bases as noted above.

2JSM in 5 μs OL15 simulation: T1, A2 and A20 triple was not stable in OL15 simulation. At 200 ns A2 moved and aligned in the groove. T1:A20 base pair was maintained throughout the simulation (Figure S23c). In the LL1, T12:A14 native Hoogsteen base pair was sampled for ~76% of the simulation time (Figure S23d) and T13 stacked below T12. In the LL2, T18 was exposed to the solvent while T19 and A20 stacked on the G-stem for the entire simulation.

2JPZ

The flanking nucleotides TTA are present at the 5'-end. The three bases are sequentially stacked over one another in the starting structure. A3 interacts with T13 and A15 of LL2 to form A3:T13:A15 triple. In LL1, T7 is oriented in the groove and held together by hydrogen bonds with G5 and its own phosphate group. T8 and A9 stack on G-stem and form a triple alignment with T25 below the G-stem. In the LL2, T13 and A15 form triple on top of the quartets while T14 stacks on T13. Among the flanking bases, T25 interacts with T8 and A9, so that they form T8:A9:T25 triple at the bottom, while T26 is stacked below it.

2JPZ in 10 μs bsc0χ_{OL4} simulation: During the bsc0χ_{OL4} simulation, T1 moved to stack with A21 in the groove containing the PL while T2 continued to stack on A3. The A3:T13:A15 triple was stable in the simulation (Figure S24a and b). T25 moved away early in the simulation and the native T8:A9 base pair was broken after 1.6 μs to form T7|T8|A9 stack which lasted until the end of the simulation. In the LL2, T13 and A15 were stabilized by the interaction with A3 while T14 stacked over the T2|A3. The 3'-flanking base T26 formed stable interactions with A9 of LL1 from 2.5 μs until the end of the simulation (Figure S24c) while T25 was exposed to the solvent.

2JPZ in 10 μs bsc0$\chi_{OL4}\varepsilon\zeta_{OL1}$ simulation: T1, T2 and A3 stack over G-stem in the starting structure but early in the simulation T1 moved towards the solvent and aligned in the groove to stack with A21 as in the bsc0χ_{OL4} simulation. The LL1 bases maintained their conformation as

in the starting structure. T7 was exposed to the solvent while T8:A9:T25 triple was mostly stable in the simulation (Figure S24e). The triple formed by LL2 bases T13 and A15 along with A3 over the G-stem was stable throughout the simulation (Figure S24d) and T14 stacked over this triple. Among the 3'-flanking bases T25 was stable and the triple it formed with LL1 was maintained throughout the simulation. T26 stacked below T25 throughout the simulation.

2JPZ in 5 µs OL15 simulation: T1|T2|A3 stacked sequentially over the G-stem. The A3:T13:A15 triple was not stable in the simulation as at 10 ns T13 moved towards the solvent. A3 and A15 continued to stack on G-stem and maintained the WC base pair (Figure S24f). In the LL1, T7 was exposed to the solvent and T8 and A9 formed T8:A9:T25 triple which was stable in the simulation (Figure S24g). In the LL2, T13 was exposed to the solvent and T14 and A15 stacked on the G-stem. The 3'-flanking base T25 stacked below the G-stem and formed the triple alignment while T26 stacked below T25.

5MVB

The LL2 of 5MVB is unstructured as the bases could not form any alignment due to the presence of the ligand on top of the G-stem, displacing the LL2 nucleotides. All the bases of LL2 are stacked over the G-stem in 2JPZ, which is an equivalent structure without the ligand.

5MVB in six 3-5 µs OL15 simulations after the ligand removal: We carried out six simulations of 5MVB without the ligand to see if the LL2 could move towards the 2JPZ conformation. The LL1 of 5MVB maintained type-1 conformation similar to the 2JPZ structure in all the simulations, as it adopts this geometry in the starting structure also.

In the first simulation, within 50 ns of the simulation start T14 and A15 of LL2 aligned over the G-stem and formed triple with A3, while T13 was exposed to the solvent. The loop thus attained type-1 conformation. ATA triple is also present in 2JPZ but instead of T14, T13 is present in the triple in 2JPZ. The triple lasted until 700 ns and then A15 moved towards the solvent. T14:A3 Hoogsteen base pair was stable until the end of the simulation and type-2 was the most sampled conformation of the LL2 (Figure S11b).

In the second simulation, all the bases of the LL2 arranged to stack over the G-stem. A15 formed Hoogsteen base pair with T13 and T14 stacked over T13 for initial 300 ns. The flanking bases did not interact with LL2 as T2|A3 stack aligned in the groove while T1 aligned in the other groove. LL2 bases rearranged after 300 ns as T13 moved towards the solvent and stable T14:A15 Hoogsteen base pair was formed. Thus type-1 was the most sampled conformation of the LL2 in the second simulation (Figure S11c).

In the third simulation, type-3 was the major conformation of the LL2 as T13 and A15 moved to stack over the G-stem within the first 50 ns of the simulation (Figure S11d). T13 formed a single hydrogen bond with 5'-flanking base A3 and its methyl group oriented towards the G-stem channel. T14 was exposed to the solvent and sampled T1(H6)-T14(O2) bond.

In the fourth simulation, A15 moved to stack over G-stem within 20 ns of the start of the simulation and formed stable *trans* WC base pair with A3. T14 stacked over A15 and T13 was exposed to the solvent for the entire simulation time. T1|T2|A3 stack similar to 2JPZ was sampled in this simulation. Also, T2 formed a symmetric base pair with T14 of the LL2. Type-1 was the stable conformation of LL2 in this simulation (Figure S11e).

In the fifth simulation, A15 moved to stack over the G-stem early in the simulation and formed hydrogen bonds with A3. T13|T14 stack was exposed to the solvent and at ~2.4 μs T14 arranged to stack over A15. The LL2 eventually attained type-1 conformation (Figure S11f). T1 was stacked over the T14|A15 stack while T2 was exposed to the solvent.

In the sixth simulation, all the three flanking bases T1|T2|A3 stacked over G-stem as in 2JPZ. Early in the simulation, T13 stacked over G12 while T14 stacked with T1. A15 was trapped in the groove due to G11(O3')-A15(H61) hydrogen bond which lasted throughout the simulation (Figure S11g). T13 formed base pair with T2 but it was not planar in all the frames. The LL2 could not attain any of our four basic loop types in this simulation even after 5 μs.

Comparison of experimental NMR NOE data with the simulation ensembles

We compared the NMR restraints with higher degree of confidence (upper bound < 6 Å) of structures 2KF8, 2MBJ, 2GKU and 2JSM with the weighted average of the NOE distances in the respective simulation ensembles (Tables S3-S6). The proton-pairs in which weighted-average NOE distance in simulations were more than the NMR upper-bound values were investigated along the trajectories. The distance violations are considered major when the weighted-average values in simulations and NMR upper-bound value is ≥ 0.5 Å. The analysis was done using supertrajectories (superensembles) formed by joining all the simulation trajectories of the respective PDB structure into one. All NOEs relevant for the studied loops and flanking nucleotides were considered.

2KF8: In 2KF8, inter-proton distances of high-confidence were maintained in the simulations and no major violation was observed (Table S3). Minor violation was observed for A18(H2) and T5(H1') proton-pair. T5 stacks below G3 of A6:G3:A18 triple in the starting structure but in ~28% of the simulation frames, G3|T4|T5 stack was sampled. A18(H2) and T5(H1') proton distance was increased in such an arrangement. In other frames as well, T5 was flexible as has been discussed in the main text and above in the Supporting information description of the individual trajectories.

2MBJ: The list of relative weighted average of the NOE distances in the simulation superensembles with respect to the NMR upper-bound distance of 2MBJ is presented in the Table S4 and the observed major violations are analyzed below.

Major violations

[A3(H2) and A21(H2)] and [T20(H2', H2") and A21(H8)]: LL2 of 2MBJ is in type-2 conformation and its A21 can potentially form a triple with A3:T20. Interactions of A21 with A3 and T20 were observed in one (bsc0χ_{OL4} simulation) out of five simulations (Table 3). In the bsc0χ_{OL4} simulation, χ angle of A21 moved from *anti* to *high-anti* region and A21 oriented itself such that A21(H2) and A21(H8) are farther away from A3(H2) and T20(H2', H2"), respectively (Figures S30 and S31). In all the other simulations, A21 moved and aligned towards the groove

(Figures S30 and S31). These deviations of A21 from the starting position account for the violations in distances between A3(H2) and A21(H2) and T20(H2', H2") and A21(H8) (Table S4).

2GKU: The list of relative weighted average of the NOE distances in the simulation superensembles with respect to the NMR upper-bound distance of 2GKU is presented in the Table S5 and the observed violations are analyzed below.

Major violations

T13(H1') and A14(H4'): The residues T13 and A14 belong to the LL1 of 2GKU which is in type-2 conformation in the starting structure as T12 and A14 are exposed to the solvent while T13 is stacked below the G-stem. As mentioned in the main text, LL1 of 2GKU changed to type-1 or type-4 in the simulations (Table 2). A14 moved from its solvent-oriented position to stack below the G-stem in all the simulations and the backbone rearrangement resulted in the increase in the T13(H1') and A14(H4') distance (Figure S32).

T18(H1') and T19(H4'): LL2 of 2GKU is in type-1 conformation. There was no change in conformation of this loop but T18 was flexible and showed a deviation from the starting position. T18 is exposed to the solvent in the starting structure but during the simulations, T18 oriented in the groove and its position was stabilized by hydrogen bond interaction T18(O4)-G17(H22). The weighted-average distance between T18(H1') and T19(H1') was longer than the NMR upper-bound (Figure S32 and Table S5).

T1(H6) and G9(H4'): In the starting structure of 2GKU, T1:A20 base pair is aligned over the first quartet such that T1 stacks on G9. This interaction was maintained in the simulation but while the 6-membered rings of G9 and T1 completely stack together in the starting structure, G9|T1 stacking was partial and T1 backbone was flexible in the simulations. The distance between T1(H6) and G9(H4') was increased in the simulations compared to the starting structure (Figure S32).

G21(H1) and A20(H8): A20 is aligned over G17 and G21 of the first quartet in the starting structure. During the simulations, A20 shifted to sample stable G17|A20 stack and the distance between A20(H8) and G21(H1) was increased as observed in the NOE analysis of simulation ensembles (Figure S32 and Table S5).

Minor violations

[G3(H8) and T2(H4')] and [G11(H1') and T13(H4')]: T2 is present over the first quartet and although its position was maintained in the simulations, violations in the G3(H8) and T2(H4') were observed due to backbone flexibility. T13 stacks below G11 in the starting structure. As discussed in the main text and description of individual trajectories above in the Supporting Information, T12 moved to stack in between T13 and G11 for ~50% of the total simulation time. This resulted in the increase in G11(H1') and T13(H4') distance as is observed in the NOE analysis (Table S5).

2JSM: The list of relative value of weighted average NOE distances in the simulation superensembles of 2JSM is presented in the Table S6 and the observed violations are analyzed below.

Major violations

[A14(H8) and T13(H2',H2")] and [G15(H8) and A14(H5',H5")]: LL2 of 2JSM changed from type-3 to type-4 in both the bsc0$\chi_{OL4}\varepsilon\zeta_{OL1}$ and OL15 simulations as T13 oriented to stack below T12. T12 and A14 form a Hoogsteen base pair in the starting structure of 2JSM. This experimentally suggested Hoogsteen base pair switched to *trans* WC base pair in both the simulations due to the flip in backbone of A14 (Figure S23). The distance between G15(H8) and A14(H5', H5") was increased significantly in the simulations and is reflected in the relative value of weighted-average NOE distance of 2.950 Å(Figure S33 and Table S6).

Minor violations

A2(H8) and T1(H2',H2"): T1 and A2 form base triple with A20 over the first quartet in 2JSM. During the simulations, A2 oriented in the groove and its interactions with T1 and A20 were not sampled in any of the simulations. Therefore, distance between T1(H2',H2") and A2(H8) was increased and positive NOE violations were observed (Table S6).

T12(H1') and T13(H1'): The LL2 of 2JSM is in type-3 conformation as T12 and A14 stack below the G-stem while T13 is exposed to the solvent. During both the simulations of 2JSM, LL2 changed from type-3 to type-4 conformation as T13 aligned to stack below T12. As a result of movement of bases and backbone rearrangement, the distance between T12(H1') and T13(H1') was increased (Table S6).

Table S1. List of human telomeric DNA GQs observed in atomistic experiments

S.No.	Topology	PDB id	Sequence	5'-3' *syn-anti* orientation of the Gs in G-stems	Loop sequence	Stabilizing Ion in experiment
1.	Parallel-stranded	1KF1[1]	5'-AGGG(TTAGGG)$_3$-3'	5'-*aaa*--*aaa*--*aaa*--*aaa*-3'	propeller-propeller-propeller	K^+
		1K8P[1]	[5'-TAGGG(TTAGGG)T-3']$_2$	5'-*aaa*--*aaa*-3' 5'-*aaa*--*aaa*-3'	propeller propeller	K^+
2.	Antiparallel with three G-quartets	143D[2]	5'-AGGG(TTAGGG)$_3$-3'	5'-*asa*--*sas*--*asa*--*sas*-3'	lateral-diagonal-lateral	Na^+
3.	Antiparallel with two G-quartets	2KF8[3]	5'-GGG(TTAGGG)$_3$T-3'	5'-*sa*--*sa*--*sa*--*sa*-3'	lateral-diagonal-lateral	K^+
4.	(3+1) hybrid-1	2HY9[4]	5'-AAAGGG(TTAGGG)$_3$ AA-3'	5'-*saa*--*saa*--*ssa*--*saa*-3'	propeller-lateral-lateral	K^+
		2JSM[5]	5'-TAGGG(TTAGGG)$_3$-3'			K^+
		2GKU[6]	5'-TTGGG(TTAGGG)$_3$A-3'			K^+
5.	(3+1) hybrid-2	2JPZ[7], 5MVB[8]	5'-TTAGGG(TTAGGG)$_3$TT-3'	5'-*saa*--*ssa*--*saa*--*saa*-3'	lateral-lateral-propeller	K^+
		2JSL[5]	5'-TAGGG(TTAGGG)$_3$TT-3'			K^+
6.	Antiparallel (2+2)	2MBJ[9]	5'-TTAGGG(TTAGGG)$_3$TTA-3'	5'-*ssa*--*saa*--*saa*--*ssa*-3'	lateral-propeller-lateral	Na^+

Table S2. Residue identifiers of 5'-flanking bases, LL1, LL2 and 3'-flanking bases of the GQ structures investigated in the present study

PDB id	**5'-flanking bases**	**LL1**	**LL2**	**3'-flanking bases**
143D	A1	T5, T6, A7	T17, T18, A19	
2KF8		G3, T4, T5, A6	T16, T17, A18	G21, T22
2MBJ	T1, T2, A3	T7, T8, A9	T19, T20, A21	T25, T26, A27
2HY9	A1, A2, A3	T13, T14, A15	T19, T20, A21	A25, A26
2GKU	T1, T2	T12, T13, A14	T18, T19, A20	A24
2JSM	T1, A2	T12, T13, A14	T18, T19, A20	
2JPZ, 5MVB	T1, T2, A3	T7, T8, A9	T13, T14, A15	T25, T26

Table S3. Inter-residue NOE violations in the present simulations of 2KF8

PDB id	NMR upper bound (Å)	Relative value of weighted-average NOE distances in simulation ensembles (Å)[a, b]	NMR hydrogen pair[c]
2KF8	4.20	0.097	18(H2) and 5(H1')
	4.20	-1.326	15(H8) and 15(H2',H2'')
	5.64	-1.294	6(H2) and 4(C7)
	5.64	-1.205	9(H8) and 11(C7)
	4.20	-1.084	15(H8) and 18(H2',H2'')
	4.20	-0.707	15(H8) and 18(H8)
	5.64	-0.497	9(H2',H2'') and 11(C7)
	5.64	-1.357	16(H2',H2'') and 17(C7)

[a] Relative value (with respect to the upper-bound distance) of weighted-average NOE distances in simulation ensembles was calculated as $\left(\frac{1}{n}\sum_{i=1}^{n} r_i^{-6}\right)^{-1/6}$, where r_i is instantaneous distance between the two atoms in *i*-th supertrajectory frame and *n* is the total number of frames in supertrajectory, which was formed by joining all the simulation trajectories of the respective PDB structure.

[b] Violations of NOEs are indicated by positive values while negative values mean no violations. Yellow and red rows in all the NOE tables indicate minor (< 0.5 Å) and major violations, respectively.

[c] C7 in hydrogen pair refers to methyl protons of thymine

Table S4. Inter-residue NOE violations in the present simulations of 2MBJ

PDB id	NMR upper bound (Å)	Relative value of weighted-average NOE distances in simulation ensembles (Å)[a, b]	NMR hydrogen pair[c]
2MBJ	4.75	-2.216	1(H2") and 2(H6)
	5.25	-2.000	1(H5') and 21(H8)
	4.75	-1.093	3(H8)and 12(H8)
	4.75	1.666	3(H2) and 21(H2)
	4.75	-1.596	6(H2') and 9(H8)
	4.75	-1.164	6(H8)and 9(H8)
	4.75	-2.048	8(H2") and 9(H8)
	4.75	-1.167	8(H3') and 9(H8)
	5.25	-2.226	8(H2") and 9(H5')
	5.60	-3.157	8(C7) and 25(C7)
	4.75	-1.263	9(H2) and 27(H2)
	4.60	-1.679	15(H1') and 27(H8)
	4.75	-1.282	15(H2) and 27(H1')
	4.75	-1.672	18(H1') and 19(H3')
	4.25	-1.196	18(H8) and 20(C7)
	5.25	-3.109	18(H2") and 20(C7)
	4.75	0.524	20(H2',H2") and 21(H8)
	4.75	-1.075	24(H2') and 25(H6)
	3.75	-1.348	24(H2") and 25(H6)
	4.75	-0.887	24(H1') and 25(H6)
	4.75	-0.420	24(H8) and 25(H6)
	4.75	-2.009	25(H2') and 26(H6)
	4.75	-1.886	25(H2") and 26(H6)
	5.25	-2.795	25(H2") and 26(H5')
	4.75	-1.016	25(H2') and 27(H2)
	4.75	-1.410	25(H2") and 27(H2)
	4.75	-1.718	25(H1') and 27(H2)
	4.00	-0.150	6(H1) and 9(H2)
	4.00	-0.919	4(H1) and 3(H2)
	5.40	-1.777	22(H1) and 21(H8)
	4.00	-0.677	16(H1) and 15(H2)
	4.00	-0.463	10(H1) and 9(H2)
	5.40	-0.979	12(H1) and 3(H2)
	5.40	-1.199	4(H1) and 3(H1')
	5.40	-0.799	22(H1) and 21(H1')
	4.00	-0.494	18(H1) and 20(H1')
	4.00	-0.072	10(H1) and 9(H1')
	5.40	-0.201	16(H1) and 15(H2',H2")
	5.40	-0.300	10(H1) and 9(H2")

[a,b,c] Refer to footnotes of Table S3 for explanation

Table S5. Inter-residue NOE violations in the present simulations of 2GKU

PDB id	NMR upper bound (Å)	Relative value of weighted-average NOE distances in simulation ensembles (Å)[a, b]	NMR hydrogen pair[c]
2GKU	4.99	-0.966	1(H3') and 2(C7)
	4.07	-0.740	1(H1') and 2(H5')
	4.90	-0.318	1(H1') and 2(H5")
	4.68	-0.205	2(H6) and 1(H2')
	5.72	-2.659	2(H6) and 1(H1')
	5.16	-0.805	3(H8) and 2(H5')
	5.20	0.111	3(H8) and 2(H4')
	5.27	-0.022	3(H8) and 2(H5")
	5.64	0.226	11(H1') and 13(H4')
	5.64	-0.941	13(H6) and 11(H2")
	4.89	-0.970	11(H1') and 13(H5")
	3.72	-0.639	13(H1') and 14(H5')
	4.43	-0.465	13(H1') and 14(H5")
	5.07	0.515	13(H1') and 14(H4')
	4.17	-1.003	14(H8) and 13(H2', H2")
	5.97	-1.736	15(H8) and 13(H4')
	4.90	-0.460	17(H8) and 16(H3')
	3.34	-0.805	17(H8) and 16(H2")
	3.71	-0.965	17(H8) and 16(H2')
	4.32	-0.137	16(H8) and 17(H1')
	5.30	-0.795	17(H8) and 16(H1')
	5.15	-1.835	18(H6) and 17(H1')
	4.81	-1.396	17(H8) and 20(H2')
	4.31	-1.463	17(H8) and 20(H2")
	5.62	-1.746	17(H8) and 17(H1')
	4.23	-1.402	20(H8) and 17(H2')
	4.60	-1.656	20(H8) and 17(H2")
	5.75	-0.932	20(H8) and 17(H1')
	5.64	-1.854	20(H8) and 18(H2')
	4.56	-1.813	19(H6) and 18(H2")
	5.50	1.107	18(H1') and 19(H4')
	5.76	-2.064	19(H6) and 18(H3')
	5.55	-2.022	18(H1') and 19(C7)
	5.02	-0.795	19(H1') and 20(H4')
	4.49	-1.581	20(H8) and 19(H2')
	3.95	-0.996	19(H1') and 20(H5'*)
	4.13	-1.700	20(H8) and 19(H2")

Table S5 continued

2GKU	5.03	-0.997	20(H8) and 19(H3')
	5.01	-0.613	24(H8) and 23(H3')
	4.32	-1.187	24(H8) and 23(H2')
	5.51	-1.680	24(H8) and 23(H1')
	5.12	0.924	1(H6) and 9(H4')
	3.90	-0.048	3(H1) and 20(H2)
	5.20	-0.296	5(H1) and 13(C7)
	5.20	-0.151	9(H1) and 20(H2)
	3.90	-0.125	9(H1) and 1(H1')
	5.20	-1.422	11(H1) and 13(H1')
	5.20	-0.508	11(H1) and 13(H4')
	5.20	1.123	21(H1) and 20(H8)
	5.20	-2.113	21(H1) and 20(H2)
	5.20	-1.441	23(H1) and 24(H2)

[a,b,c] Refer to footnotes of Table S3 for explanation

Table S6. Inter-residue NOE violations in the present simulations of 2JSM

PDB id	NMR upper bound (Å)	Relative value of weighted-average NOE distances in simulation ensembles (Å)[a, b]	NMR hydrogen pair[c]
2JSM	4.82	-1.019	1(H1') and 2(H5')
	5.06	-0.780	2(H8) and 1(H3')
	4.45	-0.649	1(H1') and 2(H5')
	5.03	-0.540	2(H8) and 1(H1')
	4.34	0.417	2(H8) and 1(H2',H2")
	5.17	-0.784	3(H8) and 2(H5')
	5.82	-1.887	21(H8) and 2(H1')
	4.86	-0.929	12(H6) and 11(H1')
	5.81	-0.978	12(H6) and 11(H3')
	3.85	-0.412	12(H6) and 11(H2')
	4.17	-1.750	12(H6) and 11(H2")
	4.39	-1.901	13(H6) and 12(H2")
	4.64	-1.771	13(H6) and 12(H2')
	4.82	-0.794	13(H6) and 12(H1')
	4.80	0.265	12(H1') and 13(H1')
	4.86	-2.320	12(H1') and 13(H5')
	5.74	-1.140	13(H1') and 14(H5',H5")
	4.43	-0.818	14(H8) and 13(H1')
	4.37	0.822	14(H8) and 13(H2',H2")
	5.19	2.950	15(H8) and 14(H5',H5")
	4.38	-0.598	14(H2) and 23(H2')
	4.84	-1.442	14(H2) and 23(H2")
	5.19	-0.627	14(H2) and 23(H1')
	3.96	-0.817	20(H8) and 17(H2")
	5.99	-1.602	17(H8) and 20(H1')
	4.72	-1.827	17(H8) and 20(H2")
	4.58	-1.154	20(H8) and 17(H8)
	4.71	-1.237	17(H8) and 20(H2')
	4.25	-1.107	20(H8) and 17(H2")
	5.51	-1.788	19(H6) and 18(H3')
	5.88	-1.289	19(H6) and 18(H1')
	4.67	-1.698	19(H6) and 18(H2',H2")
	5.51	-0.678	19(H6) and 18(H4')
	4.66	-1.734	20(H8) and 19(H2')
	4.00	-1.177	19(H1') and 20(H5',H5")
	4.11	-1.668	20(H8) and 19(H2")
	4.91	-0.801	20(H8) and 19(H3')
	5.89	-1.320	20(H8) and 19(H1')

[a,b,c] Refer to footnotes of Table S3 for explanation

References for Supporting Information:

1. Parkinson, G. N.; Lee, M. P. H.; Neidle, S., Crystal Structure of Parallel Quadruplexes from Human Telomeric DNA. *Nature* **2002**, *417*, 876-880.
2. Wang, Y.; Patel, D. J., Solution Structure of the Human Telomeric Repeat d[$AG_3(T_2AG_3)_3$] G-tetraplex. *Structure* **1993**, *1*, 263-282.
3. Lim, K. W.; Amrane, S.; Bouaziz, S.; Xu, W.; Mu, Y.; Patel, D. J.; Luu, K. N.; Phan, A. T., Structure of the Human Telomere in K^+ Solution: A Stable Basket-Type G-quadruplex with Only Two G-tetrad Layers. *J. Am. Chem. Soc.* **2009**, *131*, 4301-4309.
4. Dai, J.; Punchihewa, C.; Ambrus, A.; Chen, D.; Jones, R. A.; Yang, D., Structure of the Intramolecular Human Telomeric G-quadruplex in Potassium Solution: A Novel Adenine Triple Formation. *Nucleic Acids Res.* **2007**, *35*, 2440-2450.
5. Phan, A. T.; Kuryavyi, V.; Luu, K. N.; Patel, D. J., Structure of Two Intramolecular G-quadruplexes Formed by Natural Human Telomere Sequences in K^+ Solution. *Nucleic Acids Res.* **2007**, *35*, 6517-6525.
6. Luu, K. N.; Phan, A. T.; Kuryavyi, V.; Lacroix, L.; Patel, D. J., Structure of the Human Telomere in K^+ Solution: An Intramolecular (3+1) G-quadruplex Scaffold. *J. Am. Chem. Soc.* **2006**, *128*, 9963-9970.
7. Dai, J.; Carver, M.; Punchihewa, C.; Jones, R. A.; Yang, D., Structure of the Hybrid-2 Type Intramolecular Human Telomeric G-Quadruplex in K^+ Solution: Insights into Structure Polymorphism of the Human Telomeric Sequence. *Nucleic Acids Res.* **2007**, *35*, 4927-4940.
8. Wirmer-Bartoschek, J.; Bendel, L. E.; Jonker, H. R. A.; Grun, J. T.; Papi, F.; Bazzicalupi, C.; Messori, L.; Gratteri, P.; Schwalbe, H., Solution NMR Structure of a Ligand/Hybrid-2-G-Quadruplex Complex Reveals Rearrangements that Affect Ligand Binding. *Angew Chem Int Ed Engl.* **2017**, *56*, 7102-7106.
9. Lim, K. W.; Ng, V. C.; Martin-Pintado, N.; Heddi, B.; Phan, A. T., Structure of the Human Telomere in Na^+ Solution: An Antiparallel (2+2) G-quadruplex Scaffold Reveals Additional Diversity. *Nucleic Acids Res.* **2013**, *41*, 10556-10562.

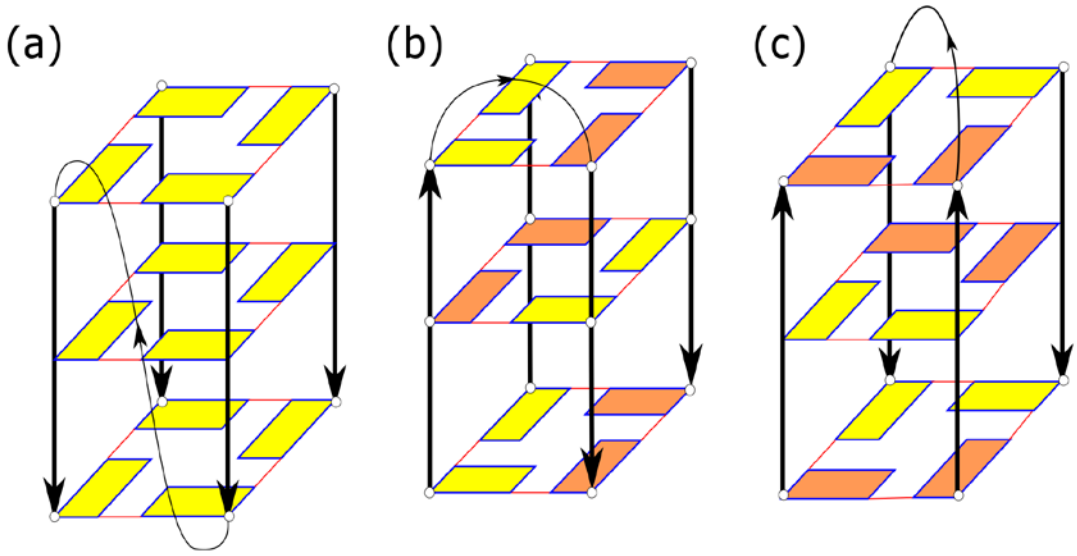

Figure S1: Topology of (a) propeller, (b) lateral and (c) diagonal loops in GQs. The yellow and orange rectangles represent *anti* and *syn* guanines, respectively. The thick and thin black lines represent the G-strands and loops, respectively, and the arrows show the directionality. Only one loop is shown in each GQ panel for clarity.

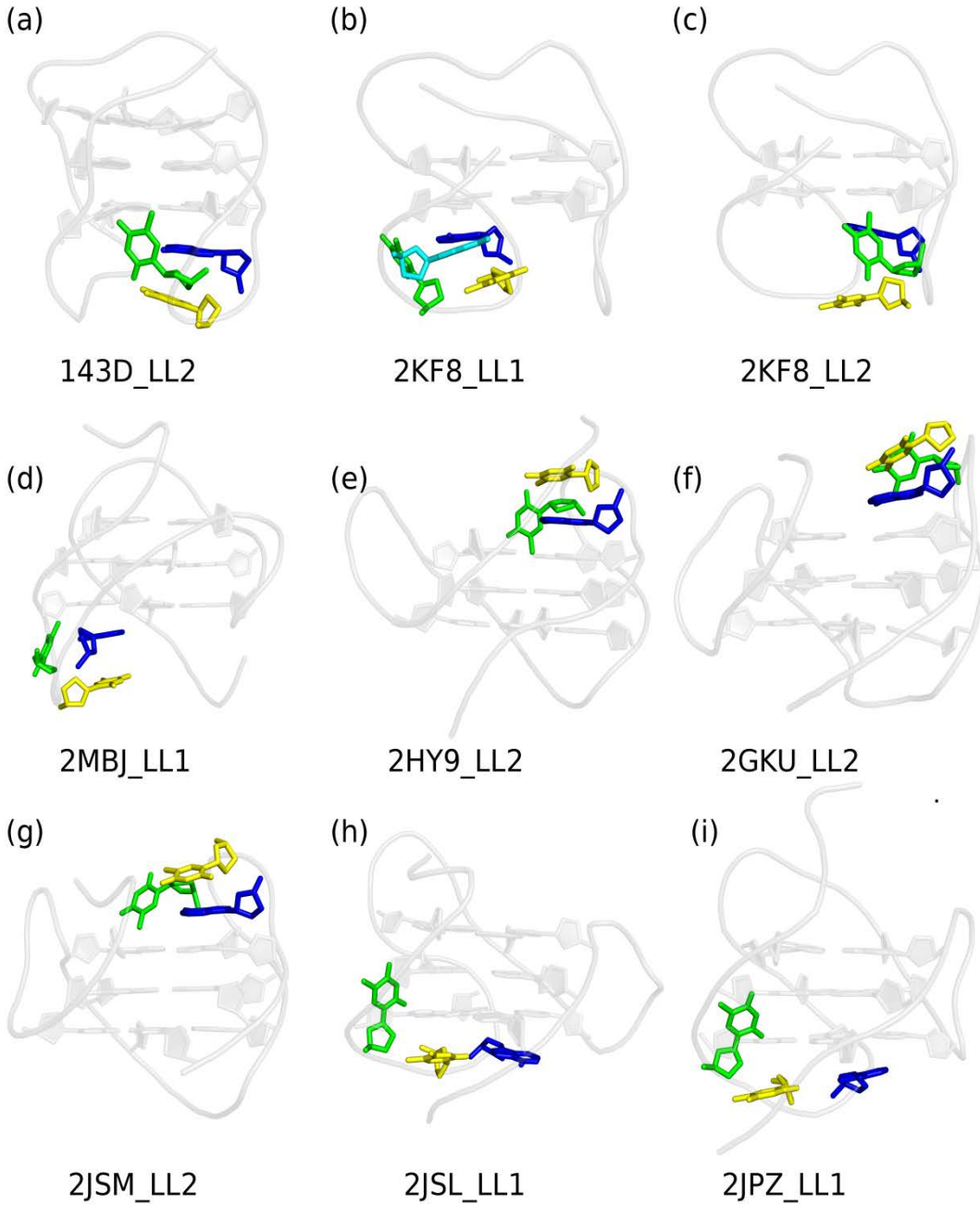

Figure S2: Representation of LLs classified as a type-1 loop arrangement. Only the G-stem, backbone and loops of interest are shown. The G-stem and backbone are shown in grey transparent cartoon. The first thymine, second thymine and adenine of the LLs are shown in green, yellow and blue, respectively. The guanine in LL1 of 2KF8 is shown in cyan.

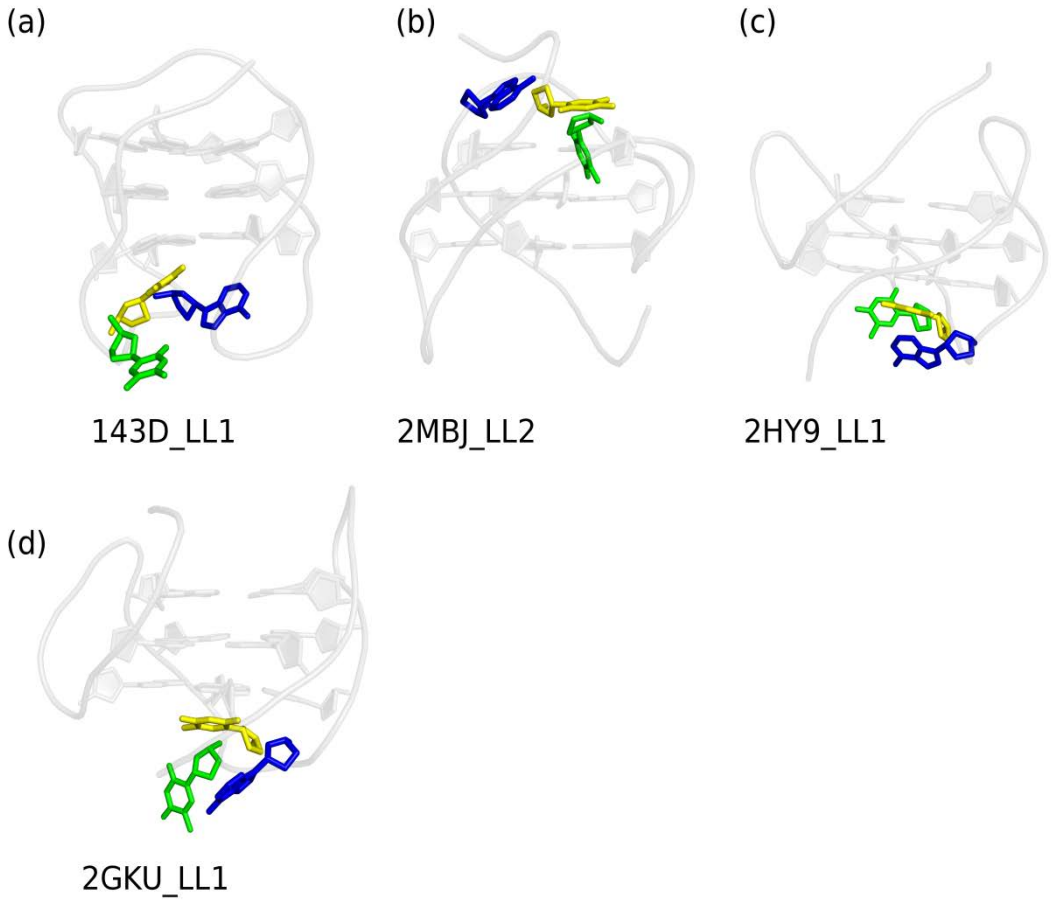

Figure S3: Representation of LLs classified as type-2 loop arrangement. Only the G-stem, backbone and loops of interest are shown. The G-stem and backbone are shown in grey transparent cartoon. The first thymine, second thymine and adenine of the LLs are shown in green, yellow and blue, respectively.

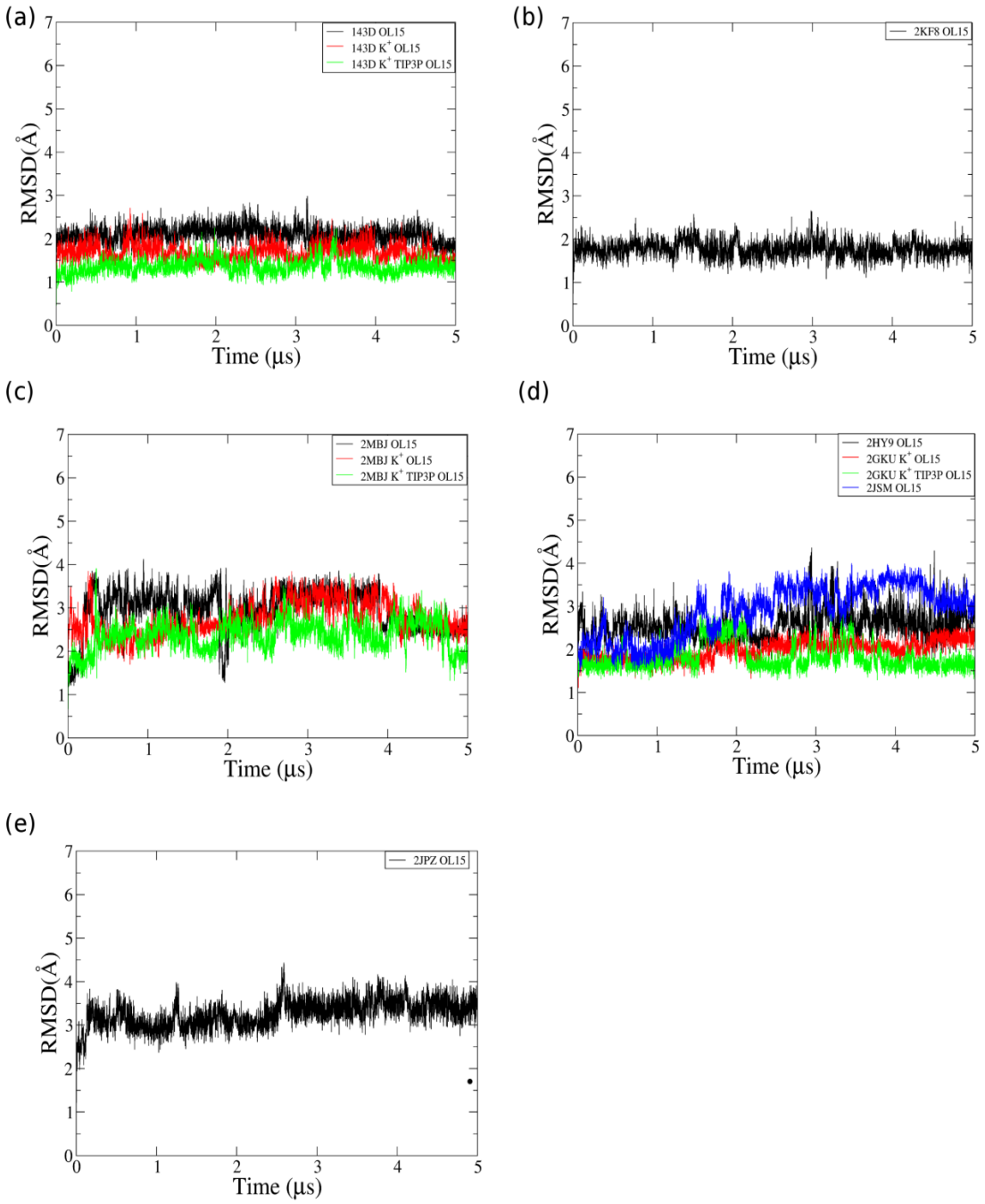

Figure S4: Backbone RMSD of the whole GQs with respect to the starting structures in OL15 simulations. The RMSDs of (a) 143D, (b) 2KF8, (c) 2MBJ, (d) 2HY9, 2GKU, 2JSM and (e) 2JPZ are shown. Na^+ and SPC/E were the general choice and K^+ and TIP3P are explicitly mentioned in the figure when used in the simulation.

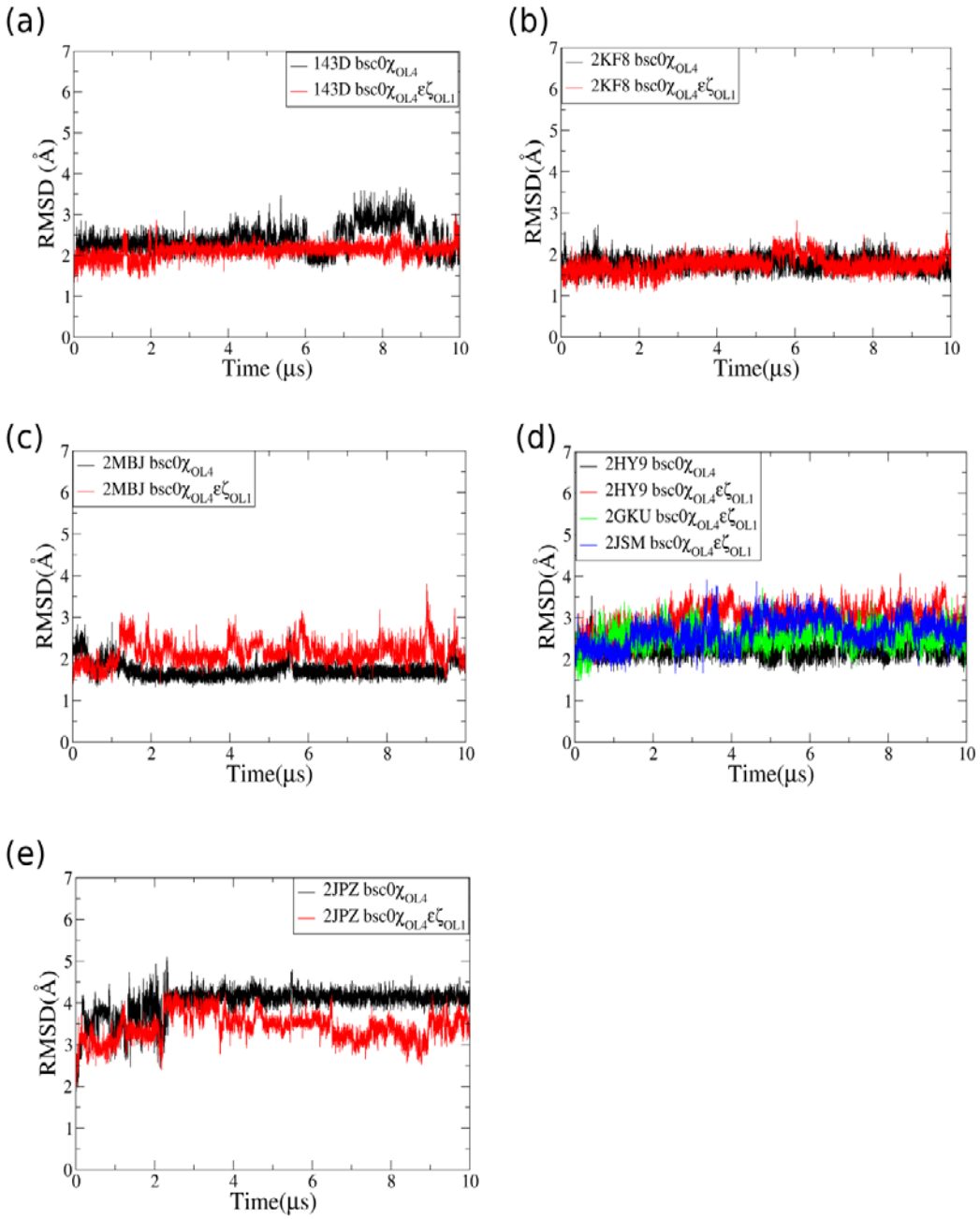

Figure S5: Backbone atom RMSDs of the whole Htel GQs in simulations with bsc0χ_{OL4} and bsc0$\chi_{OL4}\varepsilon\zeta_{OL1}$ force fields. The RMSDs of (a) 143D, (b) 2KF8, (c) 2MBJ, (d) 2HY9, 2GKU, 2JSM and (e) 2JPZ are shown.

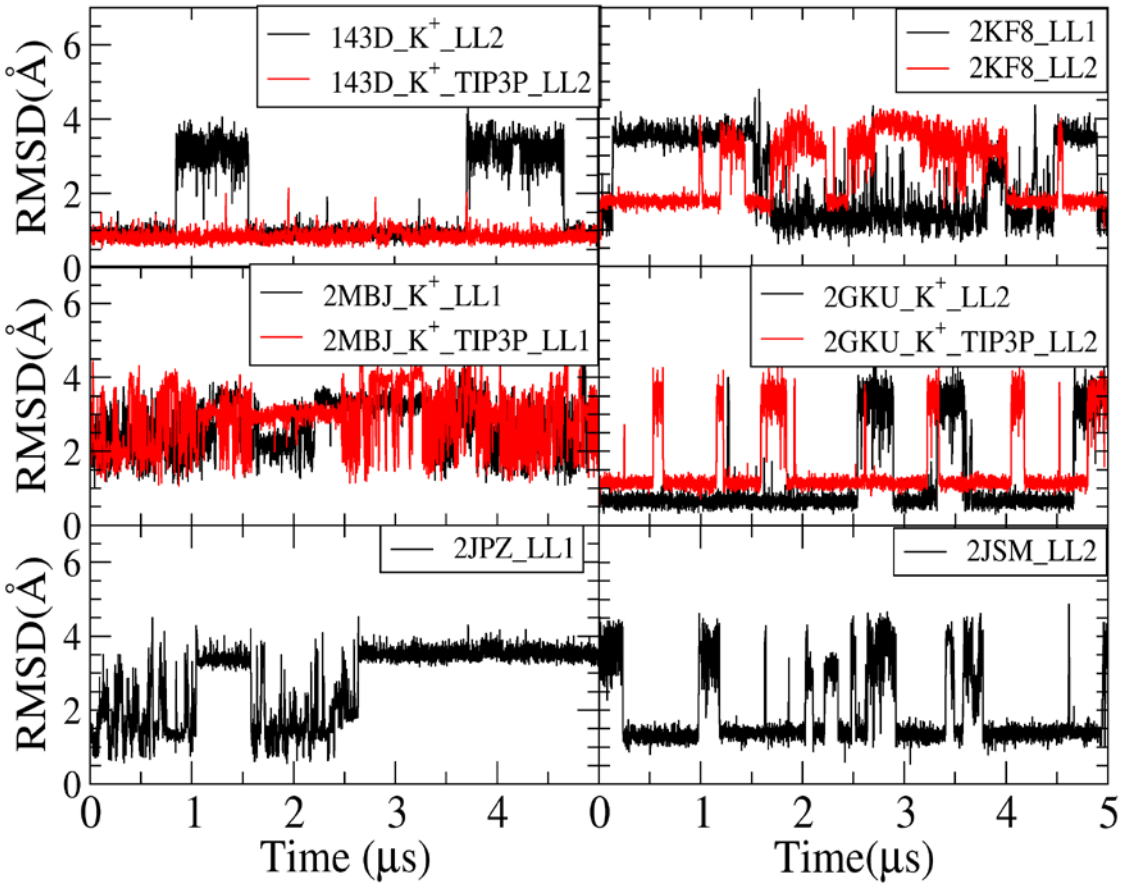

Figure S6: All-atom RMSDs of type-1 LLs of Htel GQs in the OL15 simulations in Na^+ or K^+ in SPC/E or TIP3P water model. Na^+ and SPC/E were the general choice and K^+ and TIP3P are explicitly mentioned in the figure when used in the simulation.

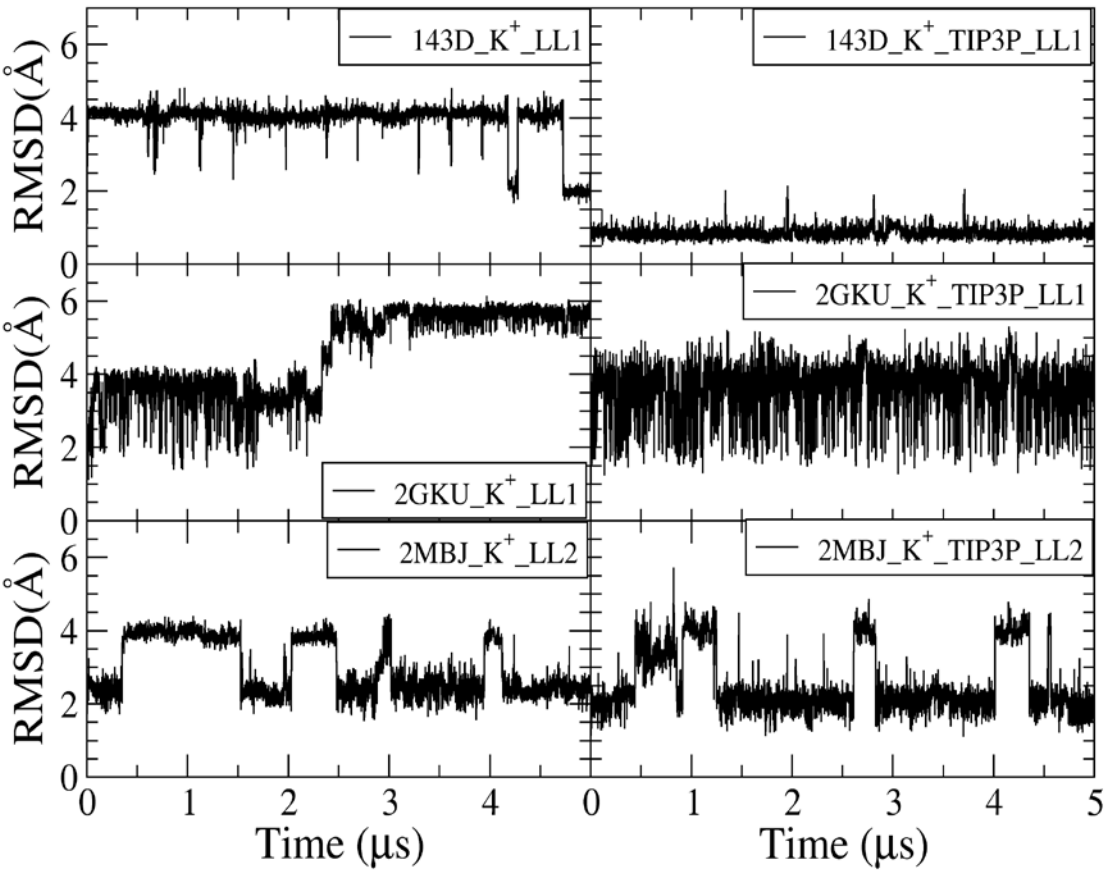

Figure S7: All-atom RMSDs of type-2 LLs of Htel GQs in the OL15 simulations in K^+ and SPC/E or TIP3P water model. SPC/E was the general choice and TIP3P is explicitly mentioned in the figure when used in the simulation.

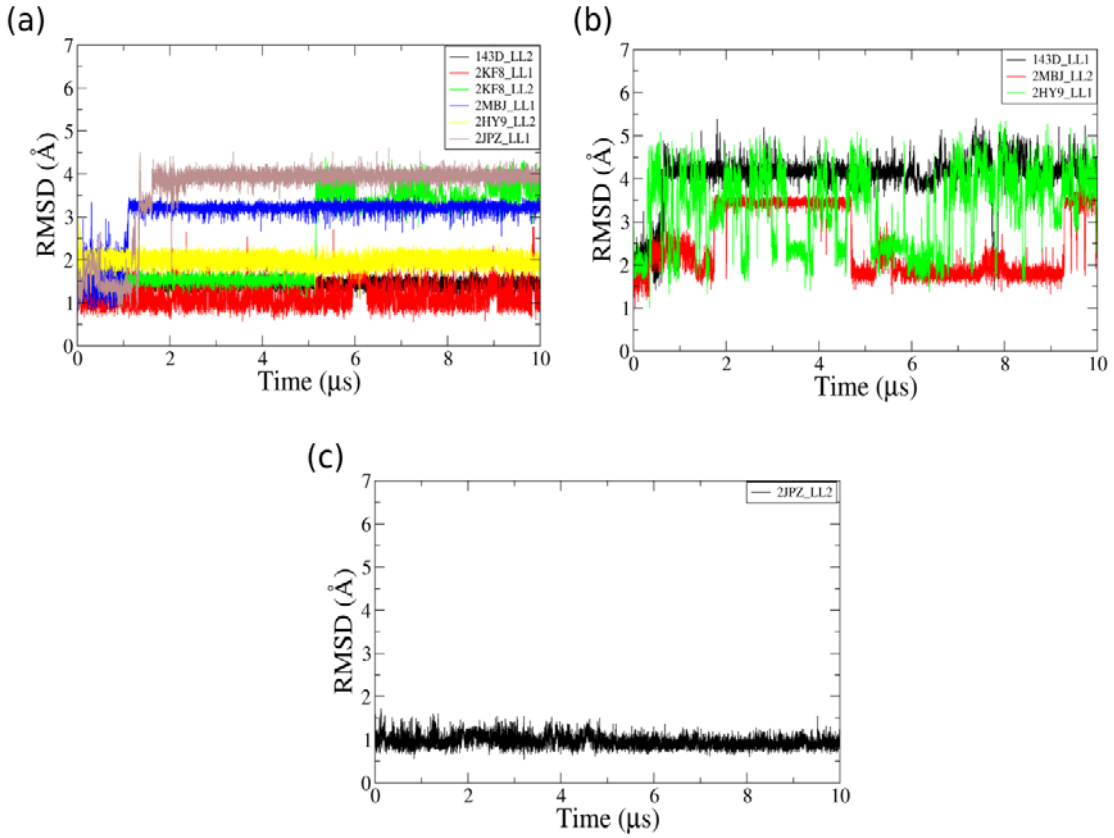

Figure S8: All-atom RMSDs of LLs of Htel GQs in the bsc0χ_{OL4} simulations. The RMSDs of (a) type-1, (b) type-2 and (c) type-4 LLs are shown.

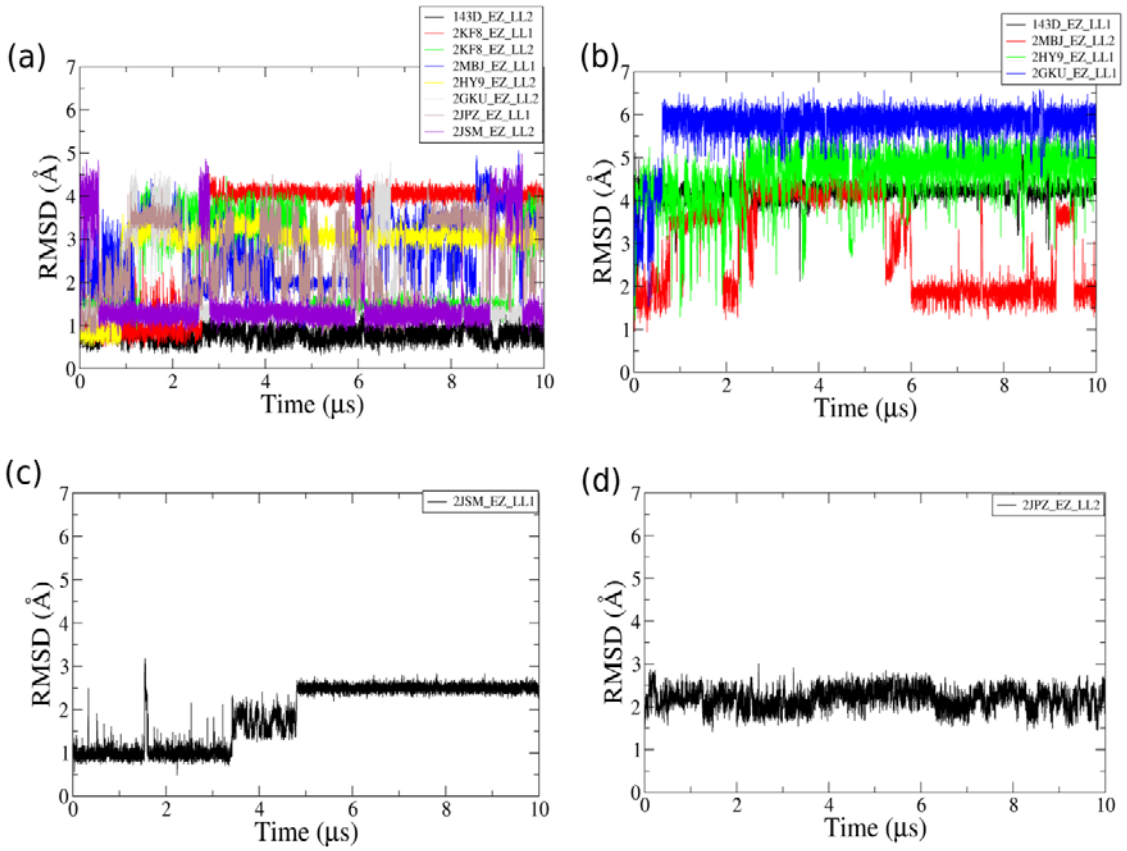

Figure S9: All-atom RMSDs of LLs in bsc0$\chi_{OL4}\varepsilon\zeta_{OL1}$ simulations. Panels (a), (b), (c) and (d) show the RMSD of type-1, 2, 3 and 4 LLs, respectively.

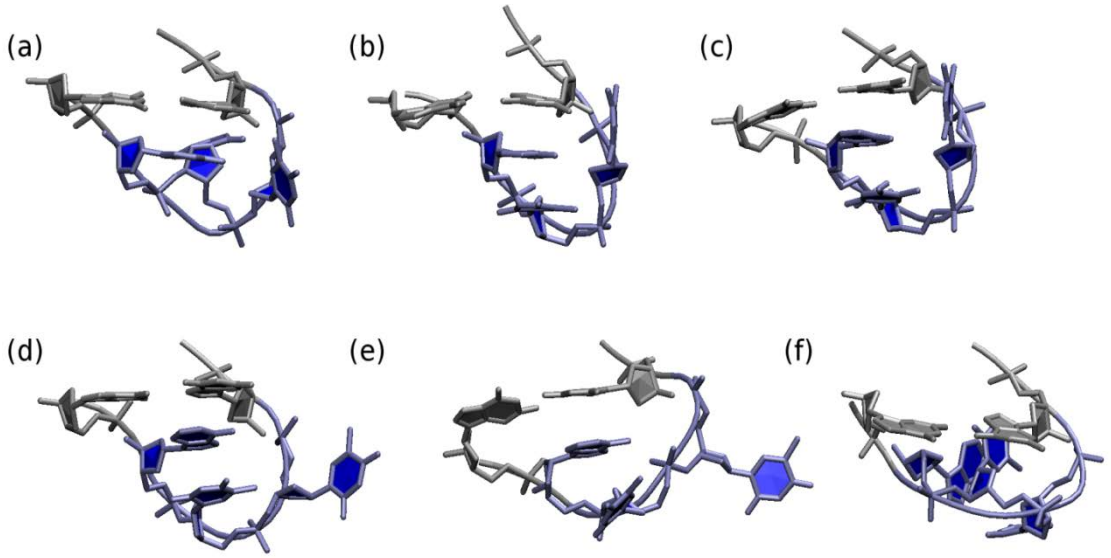

Figure S10: LL2 in 143D model 4 simulation. Panel (a) shows the starting conformation and panels (b-f) visualize the most stable (representative) conformation in five independent simulations; each panel is a representation of one independent simulation. The loop attained type-1 conformation in four out of five simulations (b-e). In the simulation represented by panel (f), LL2 did not sample any commonly observed conformation of the LL2. The TTA LLs with the preceding and following guanines are shown. The guanines and LL2 of 143D are shown in silver and blue, respectively.

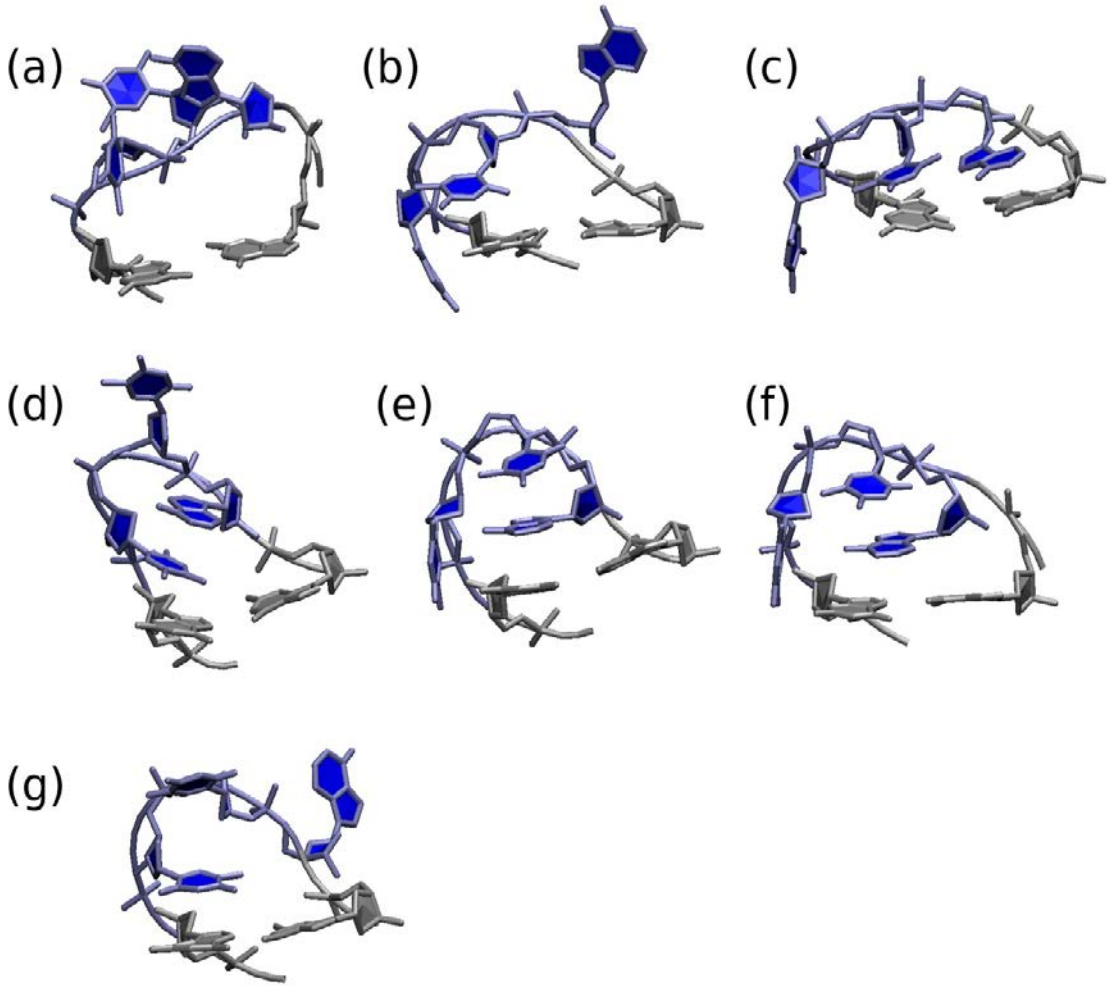

Figure S11: LL2 conformation in the multiple 5MVB simulations. The starting conformation of LL2 in 5MVB is shown in the panel (a). Panels (b-g) visualize the most stable (representative) conformation of the LL2 in six different simulations; each panel is a representation of one independent simulation. In simulations represented by panels (c, e, f) type-1 conformation was attained while panel (b) shows that the LL2 is trapped in type-2 conformation. Type-3 conformation was observed in the simulation shown in panel (d). In the simulation shown in panel (g) LL2 could not attain any of the commonly observed loop type even after 5 μs of the simulation. The TTA LLs with the preceding and following guanines are shown. The guanines are shown in silver and the LL2 is shown in blue.

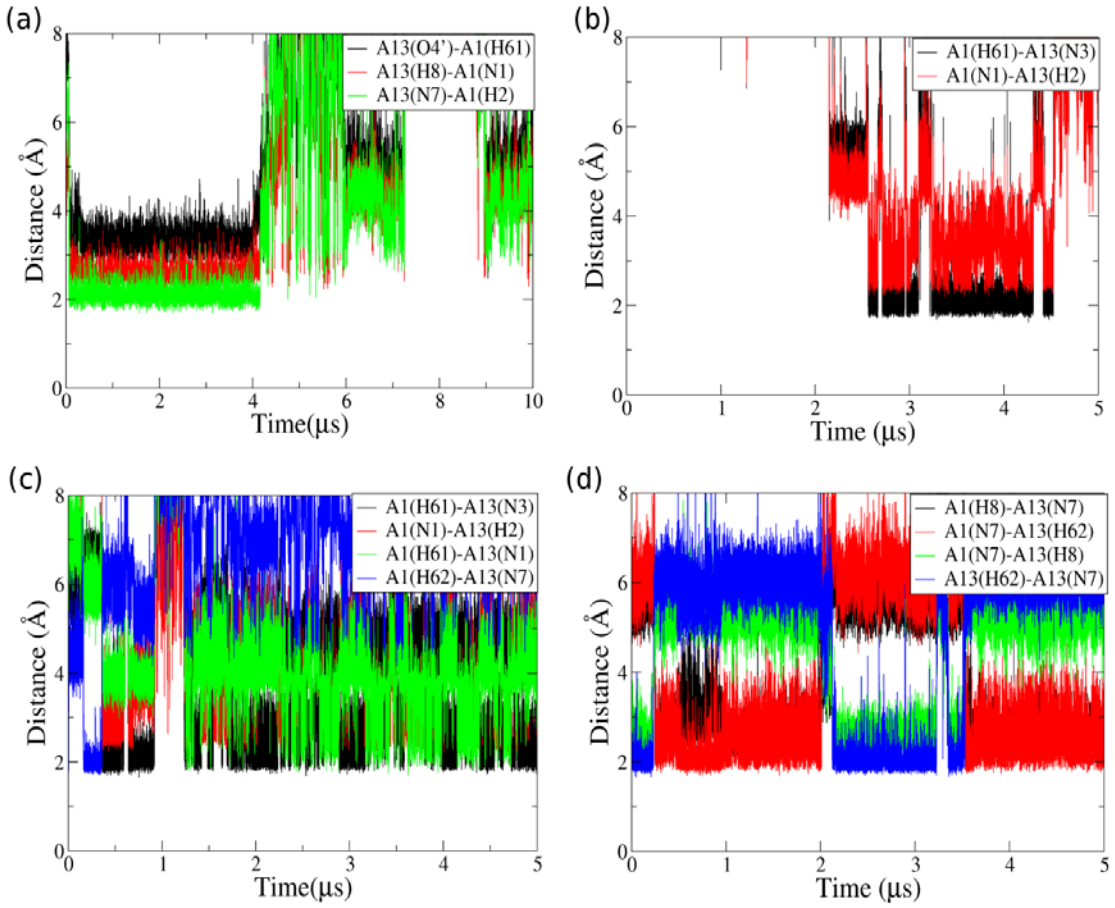

Figure S12: Distance plots to show A1 and A13 base pair interactions in 143D simulation in (a) bsc0χ_{OL4}, (b) OL15, (c) K^+/OL15 and (d) K^+/TIP3P/OL15 simulations. The A1:A13 base pair was not formed in the bsc0$\chi_{OL4}\varepsilon\zeta_{OL1}$ simulation.

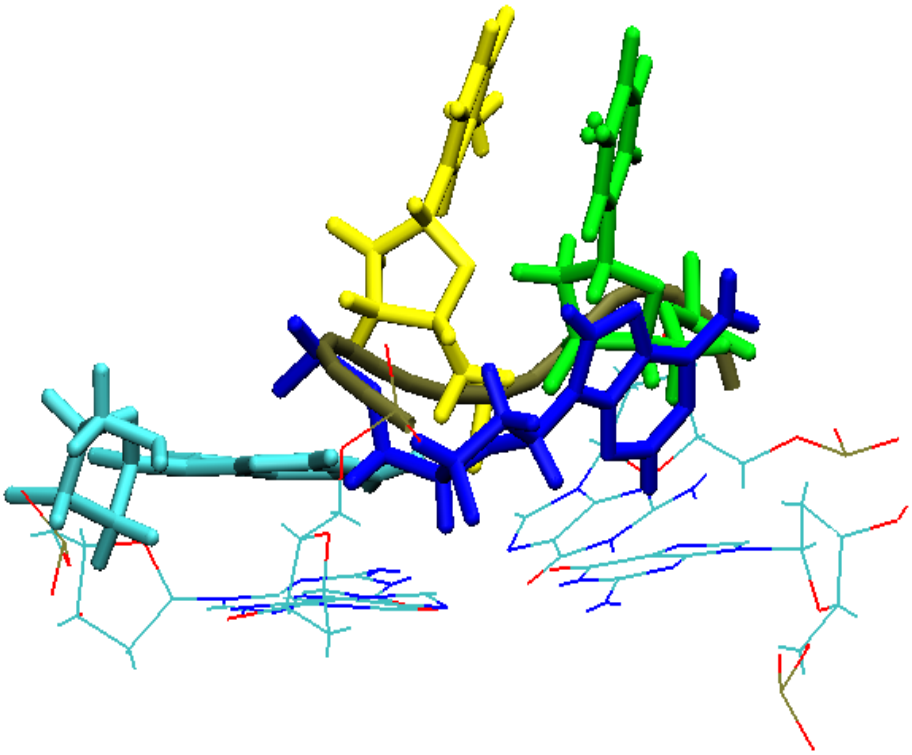

Figure S13: Arrangement within the diagonal loop of 143D in bsc0$\chi_{OL4}\varepsilon\zeta_{OL1}$ simulation. A1, T11, T12 and A13 are shown in cyan, green, yellow and blue sticks, respectively. Backbone of T11, T12 and A13 is shown as tan tube. The first quartet of the GQ is shown in lines.

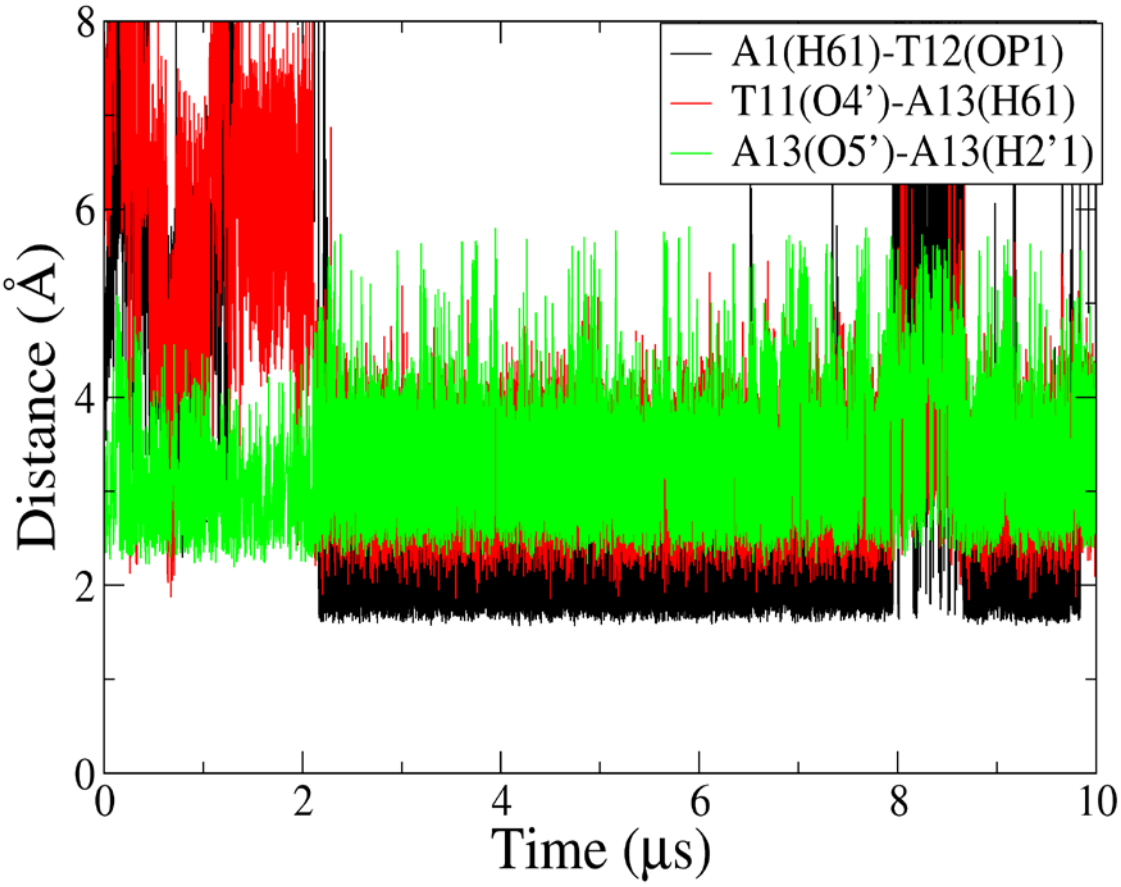

Figure S14: Distance plot to show hydrogen bond interactions within the diagonal loop of 143D in bsc0$\chi_{OL4}\varepsilon\zeta_{OL1}$ simulation that locked the loop in one conformation.

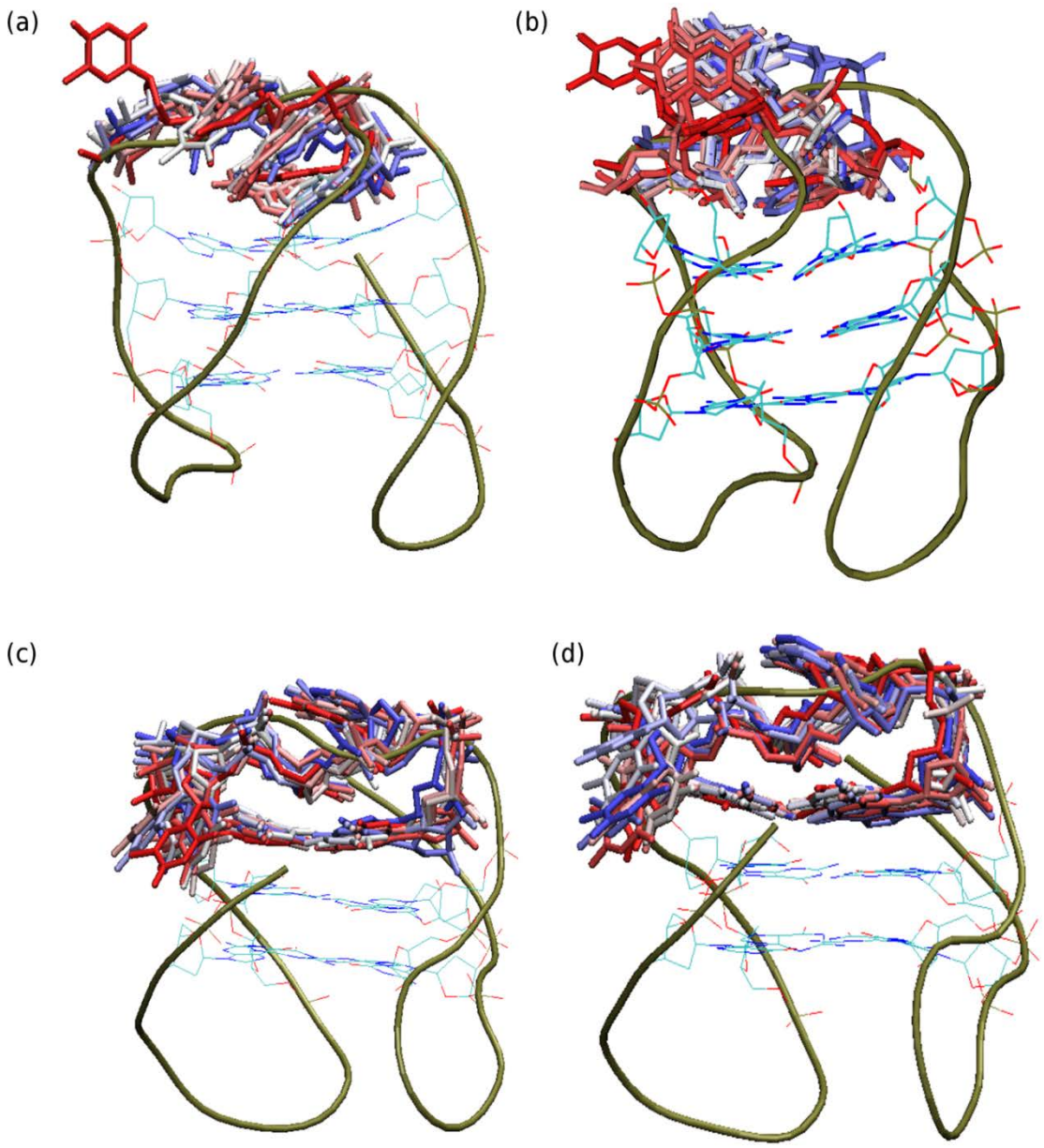

Figure S15: Representation of dynamics of diagonal loops of (a, b) 143D and (c, d) 2KF8 in 10 μs long bsc0χ_{OL4} and bsc0$\chi_{OL4}\varepsilon\zeta_{OL1}$ simulations, respectively. The backbone of GQs is shown in tan tube and G-stem nucleotides are shown in lines. The diagonal loops are shown in sticks and colored by trajectory time progression; red and blue are starting and end conformation, respectively. The diagonal loop bases are shown at time step of 1 μs.

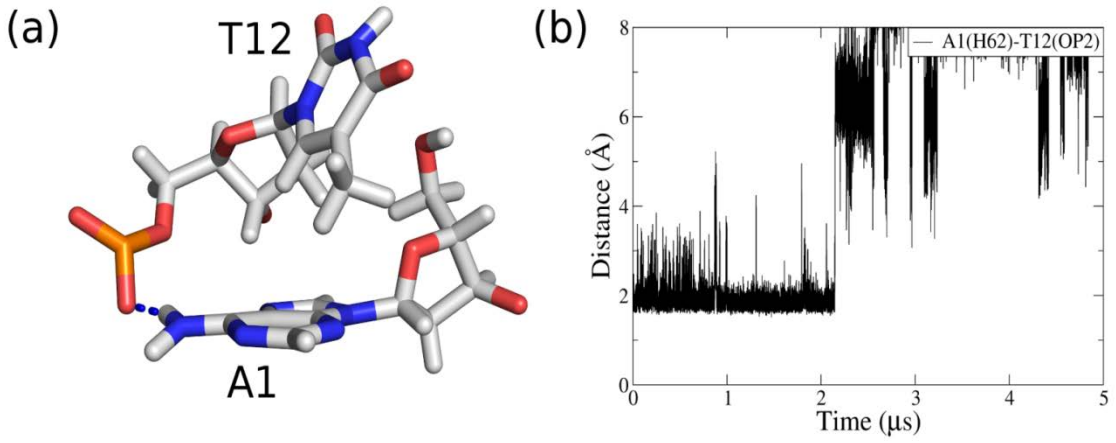

Figure S16: Interaction between A1 and T12 in 143D OL15 simulation. T12 formed CH-π and a base-phosphate interaction with A1. Panel (a) visualizes these interactions while panel (b) shows the distance plot of the base-phosphate interaction.

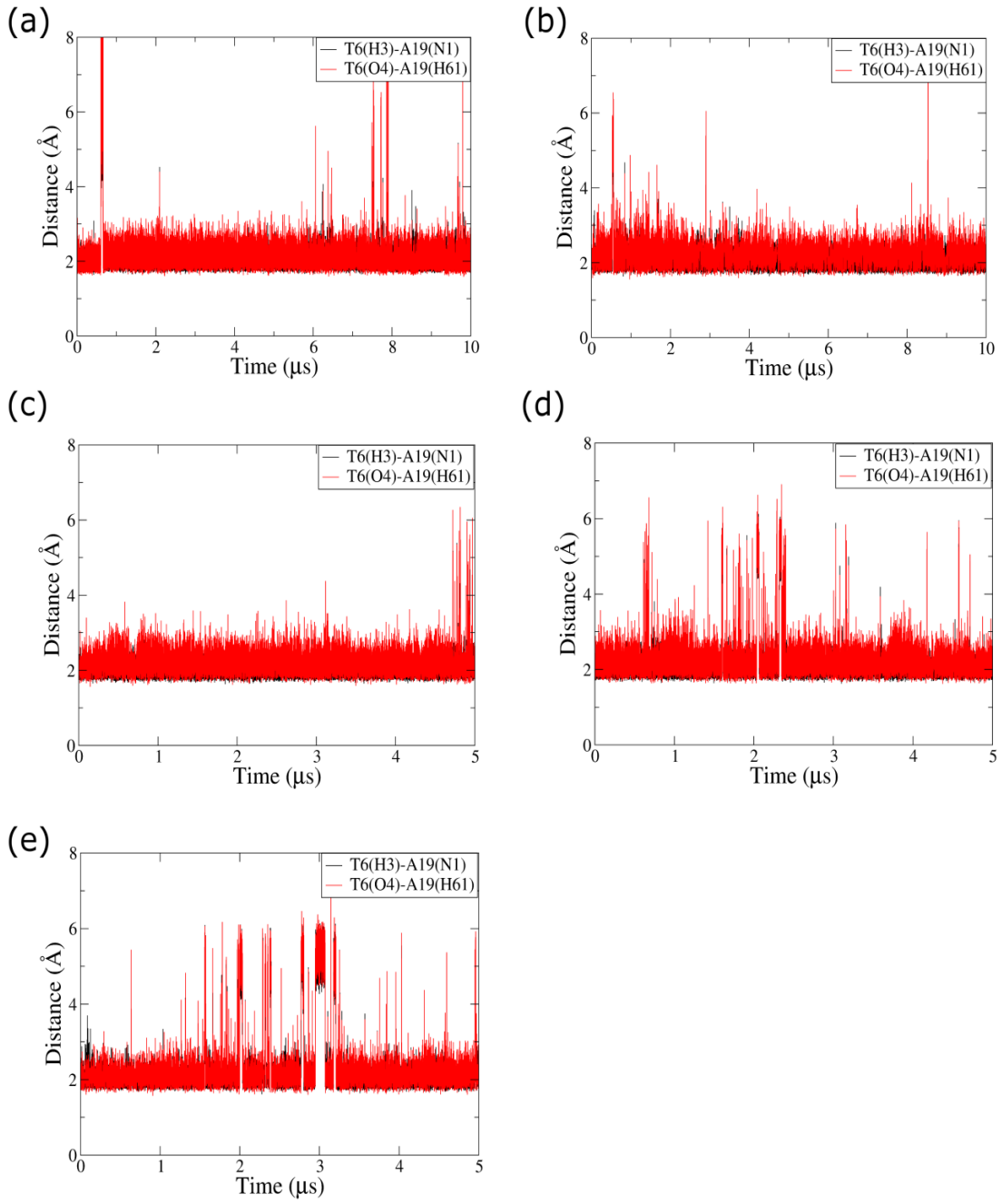

Figure S17: Distance plots of T6:A19 WC base pair in 143D in (a) bsc0χ_{OL4}, (b) bsc0$\chi_{OL4}\varepsilon\zeta_{OL1}$, (c) OL15, (d) K^+/OL15 and (e) K^+/TIP3P/OL15 simulations.

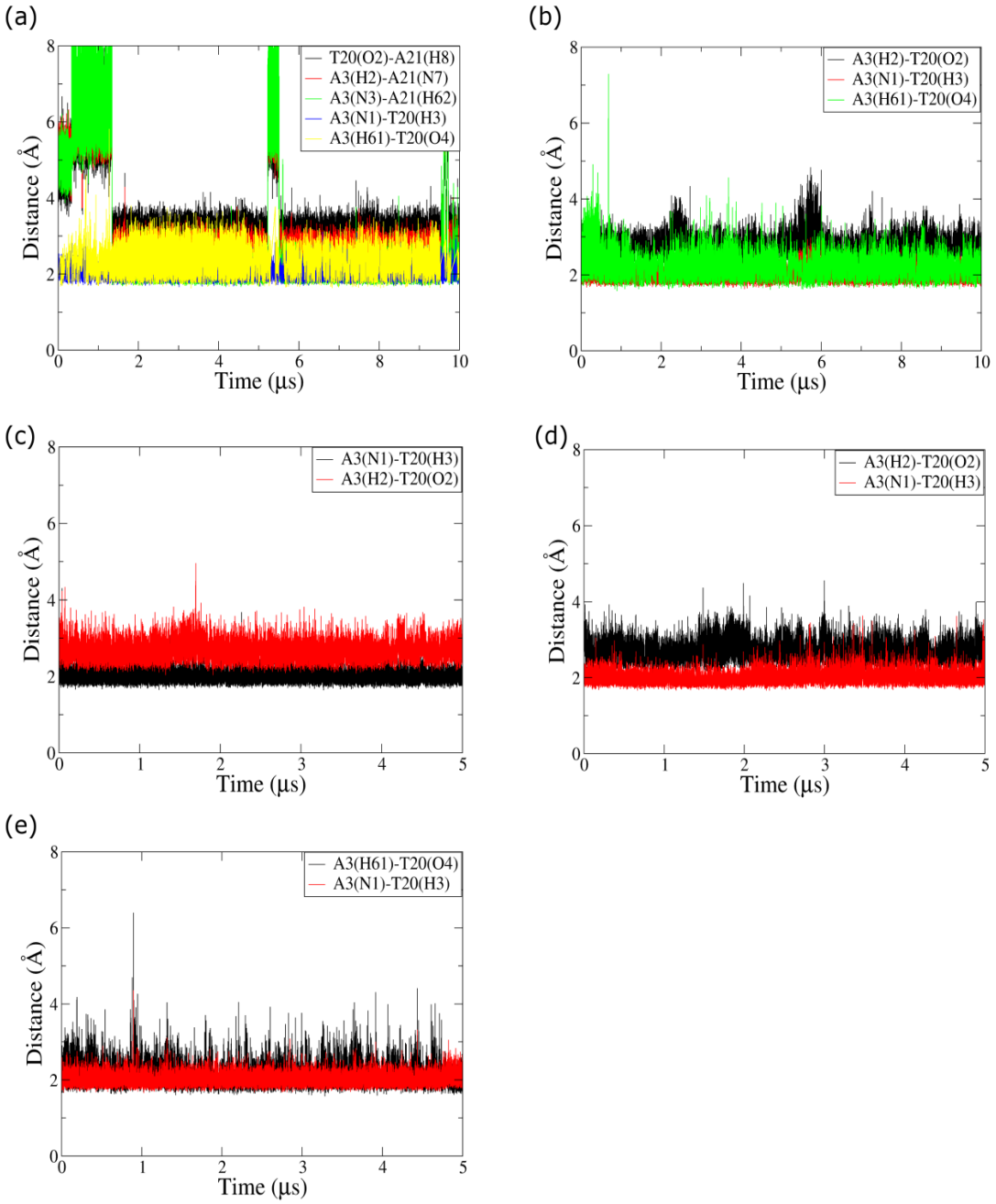

Figure S18: Distance plots of A3:T20 WC base pair in 2MBJ in (a) bsc0χ_{OL4}, (b) bsc0$\chi_{OL4}\varepsilon\zeta_{OL1}$, (c) OL15, (d) K^+/OL15 and (e) K^+/TIP3P/OL15 simulations. In bsc0χ_{OL4} simulation, A21 interacted with T20 and A3 to form the A3:T20:A21 triple.

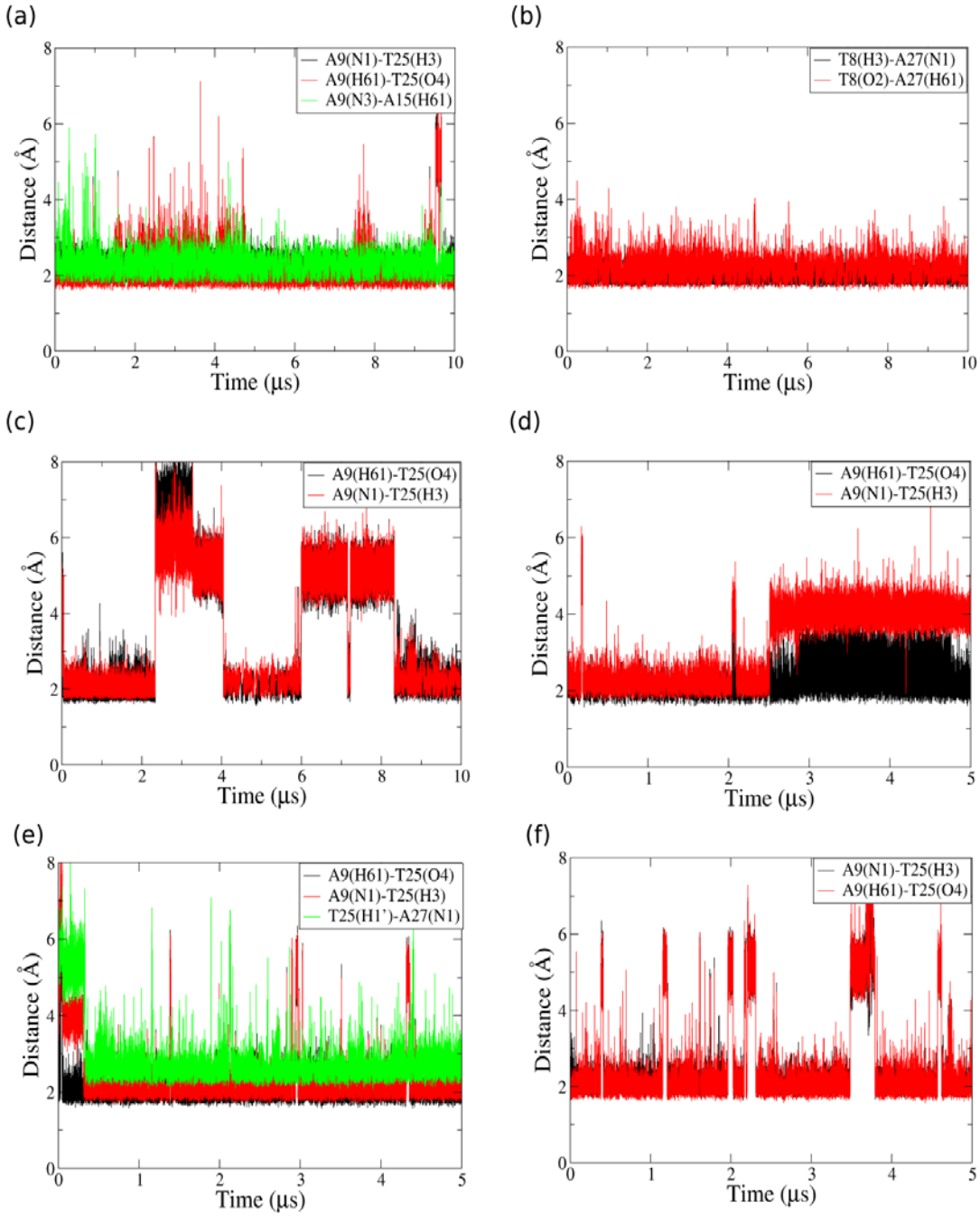

Figure S19: Distance plots of base pairs below the G-stem in 2MBJ in (a, b) bsc0χ_{OL4}, (c) bsc0$\chi_{OL4}\varepsilon\zeta_{OL1}$, (d) OL15, (e) K^+/OL15 and (f) K^+/TIP3P/OL15 simulations. In bsc0χ_{OL4} simulation, a triple was sampled as A15 aligned with A9:T25. In addition, T8:A27 base pair was formed below this triple while A9:T25 base pair was formed in all the other simulations. In K^+/OL15 simulation, flanking base A27 could interact with T25 to sample the A9:T25:A27 triple (shown in e).

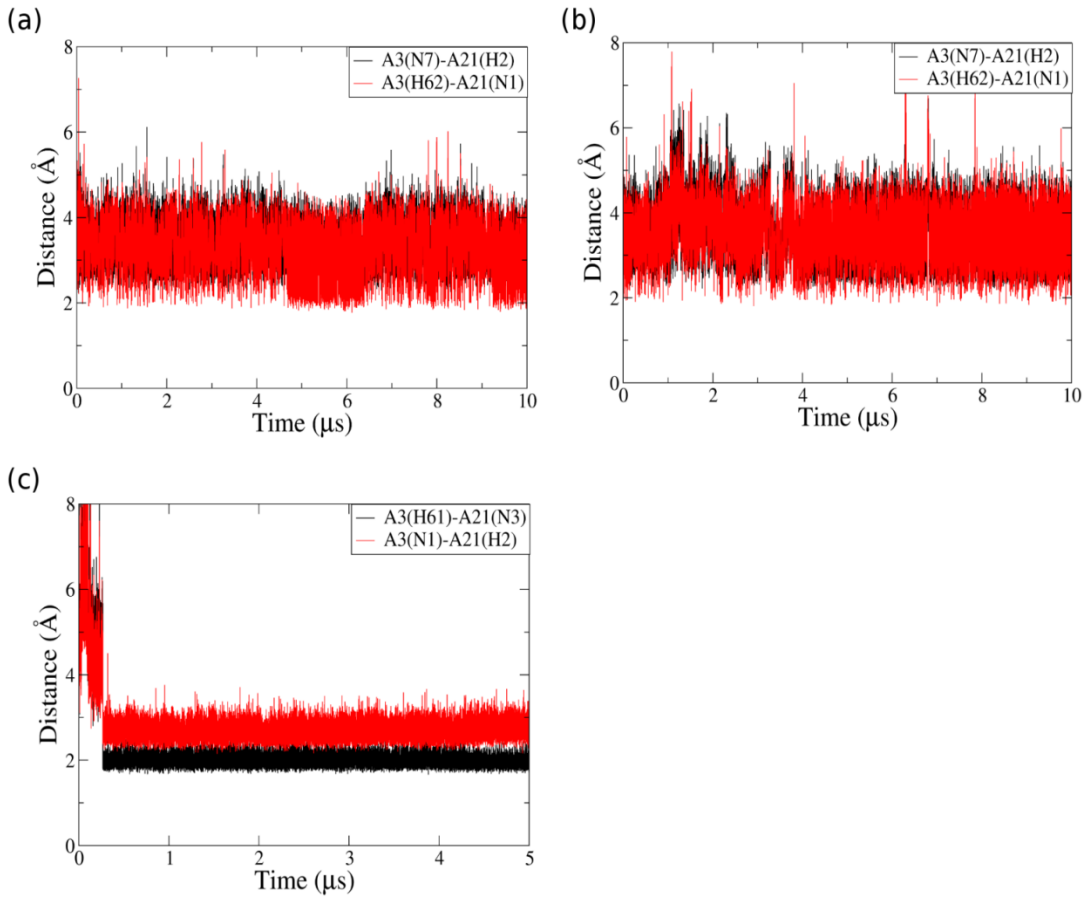

Figure S20: Distance plots of the A3:A21 base pair of 2HY9 in (a) bsc0χ_{OL4}, (b) bsc0$\chi_{OL4}\varepsilon\zeta_{OL1}$ and (c) OL15 simulations.

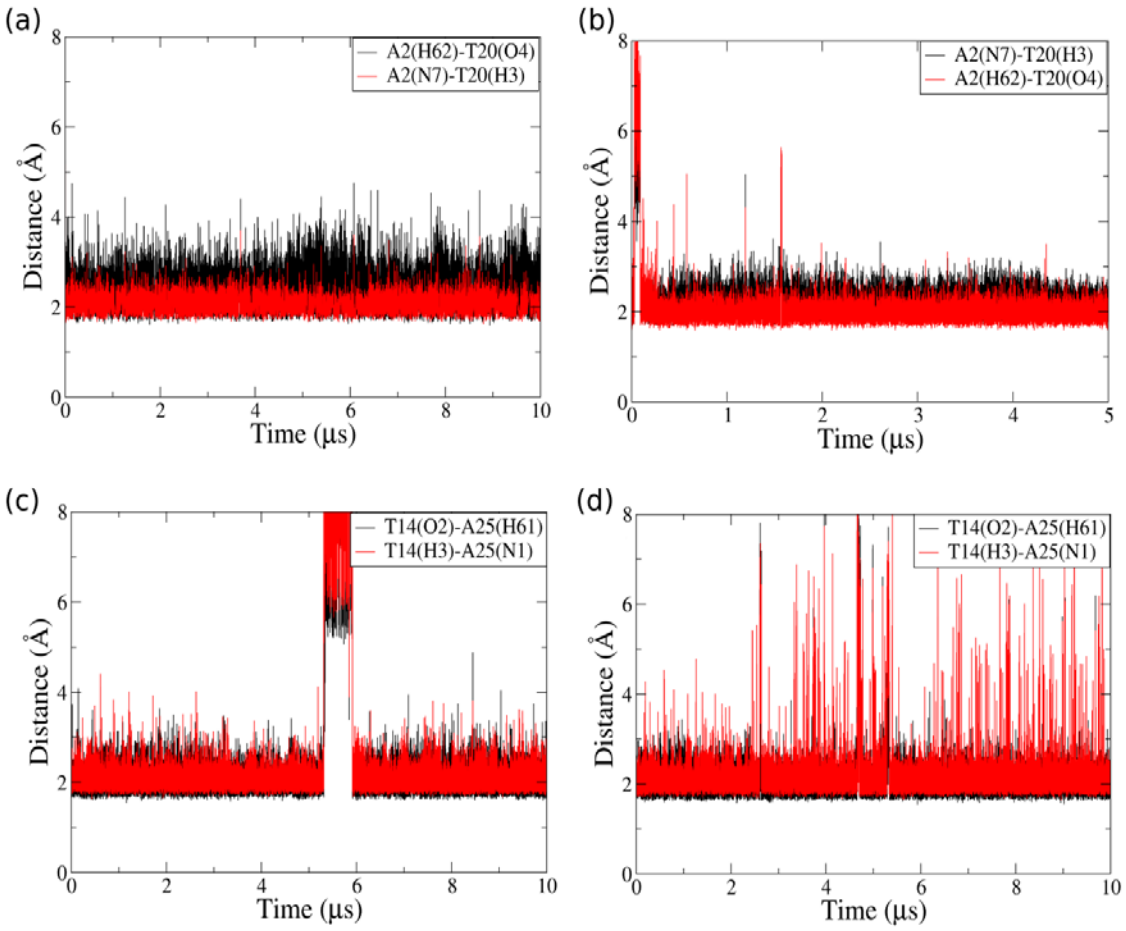

Figure S21: Distance plots of AT base pairs sampled in 2HY9 simulations. A2:T20 formed Hoogsteen base pair and it was sampled in (a) bsc0χ_{OL4} and (b) OL15 simulations. The native T14:A25 *trans* WC base pair was sampled in (c) bsc0χ_{OL4} and (d) bsc0$\chi_{OL4}\varepsilon\zeta_{OL1}$ simulations.

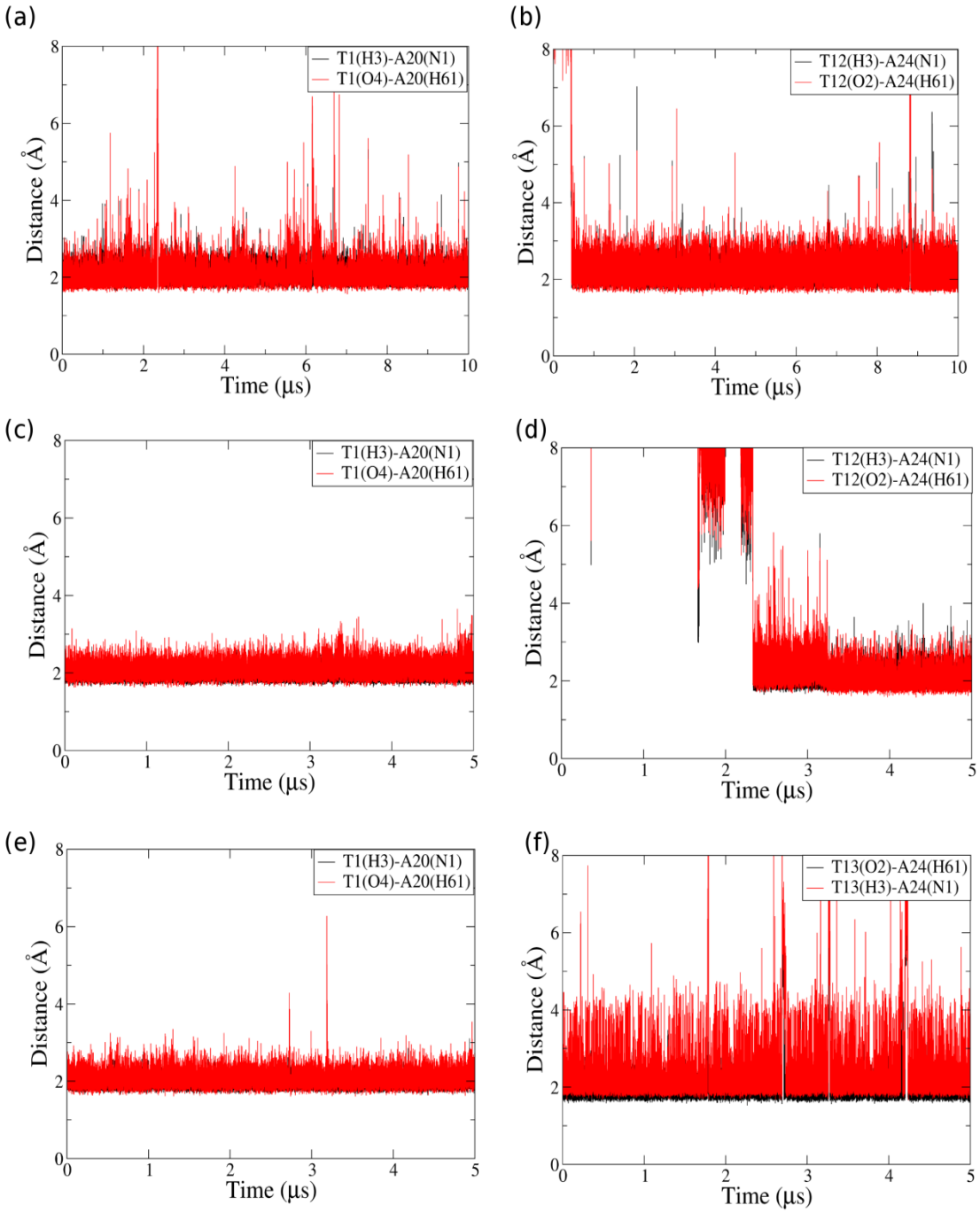

Figure S22: Distance plots of 2GKU AT WC base pairs present both above and below the G-stem. (a, b) bsc0$\chi_{OL4}\varepsilon\zeta_{OL1}$, (c, d) K^+/OL15 and (e, f) K^+/TIP3P/OL15 simulations are shown above. The T1:A20 base pair was stable in all force fields. The native (starting) T13:A24 base pair was mostly sampled in simulation with K^+ and TIP3P water model with OL15 force field and instead T12:A24 base pair was sampled in the remaining two simulations.

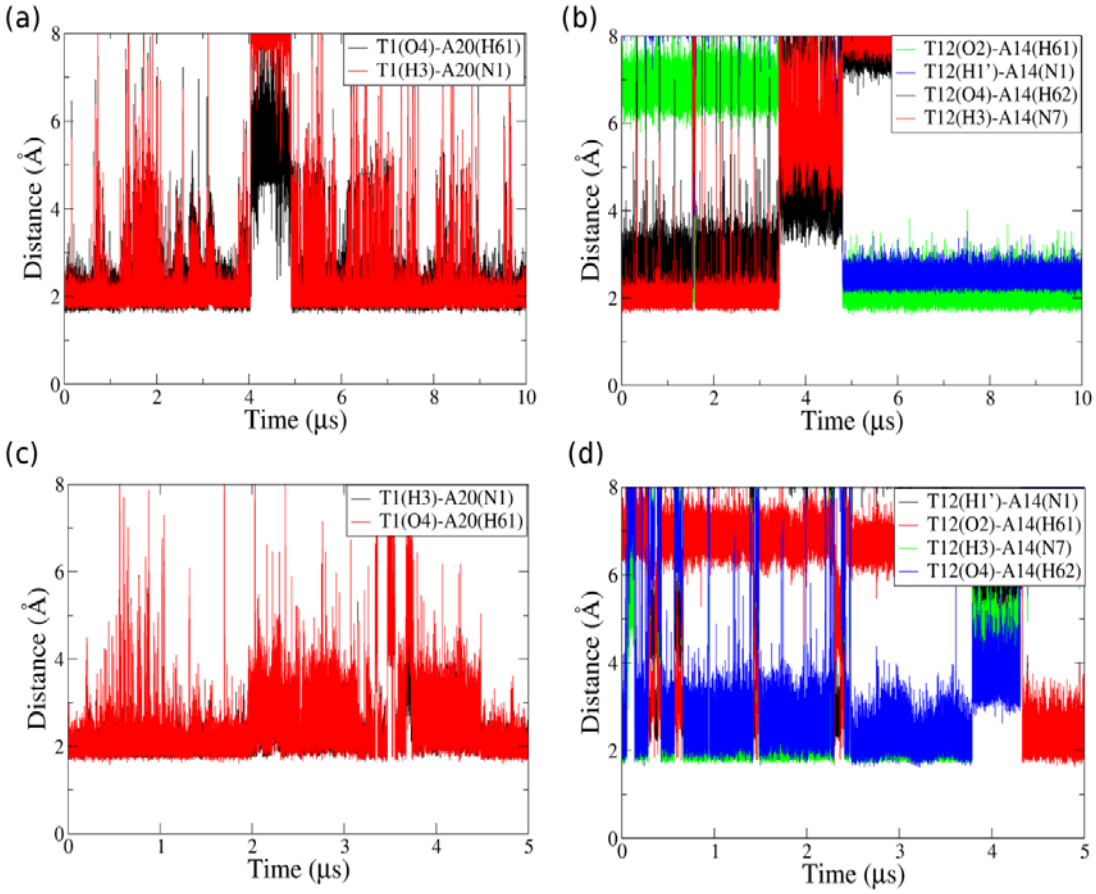

Figure S23: Distance plots of 2JSM native AT base pairs sampled in the (a, b) bsc0$\chi_{OL4}\varepsilon\zeta_{OL1}$ and (c, d) OL15 simulations. The T1:A20 WC base pair was stable in both force fields. The experimentally-suggested T12:A14 Hoogsteen base pair switched to WC base pair in both simulations.

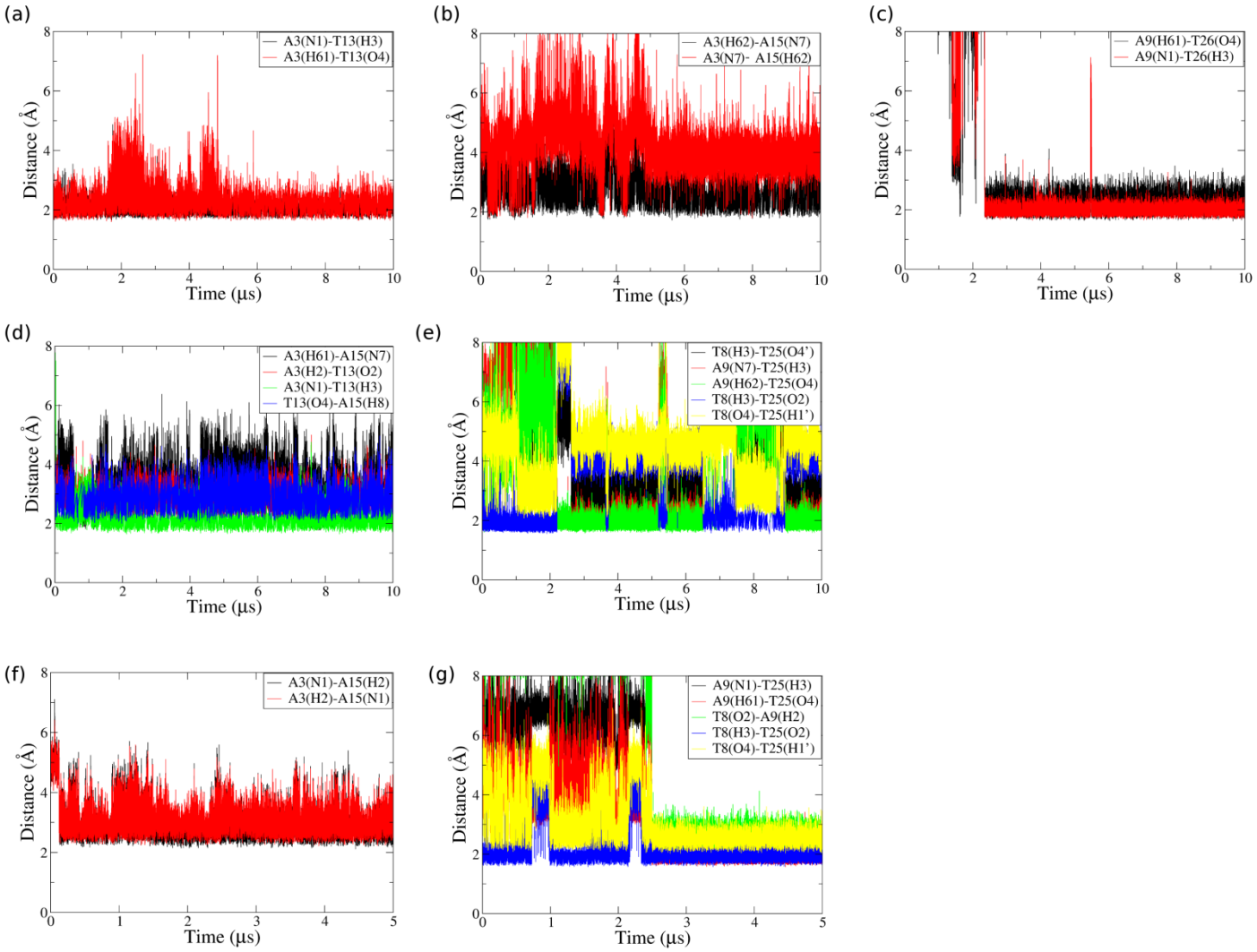

Figure S24: Distance plots of base interactions in 2JPZ in (a, b, c) bsc0χ_{OL4}, (d, e) bsc0$\chi_{OL4}\varepsilon\zeta_{OL1}$ and (f, g) OL15 simulations. A3:T13:A15 triple was stable in bsc0χ_{OL4} and bsc0$\chi_{OL4}\varepsilon\zeta_{OL1}$ simulations while A3:A15 base pair was observed in OL15 simulations. Below the G-stem, A9:T26 WC base pair was observed in bsc0χ_{OL4} simulation while in the bsc0$\chi_{OL4}\varepsilon\zeta_{OL1}$ and OL15 simulations T8:A9:T25 triple was sampled.

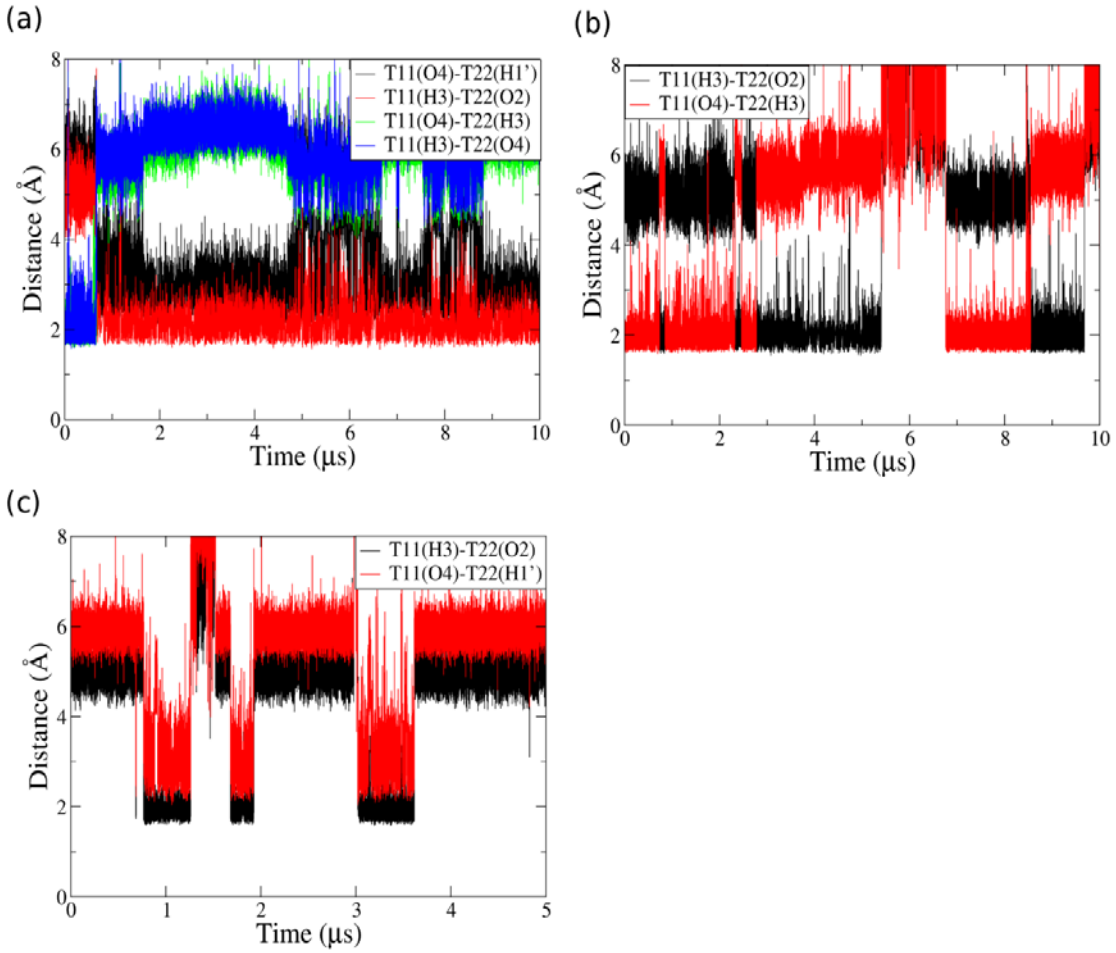

Figure S25: Distance plots of T11:T22 base pair in 2KF8 in (a) bsc0χ_{OL4}, (b) bsc0$\chi_{OL4}\varepsilon\zeta_{OL1}$ and (c) OL15 simulations.

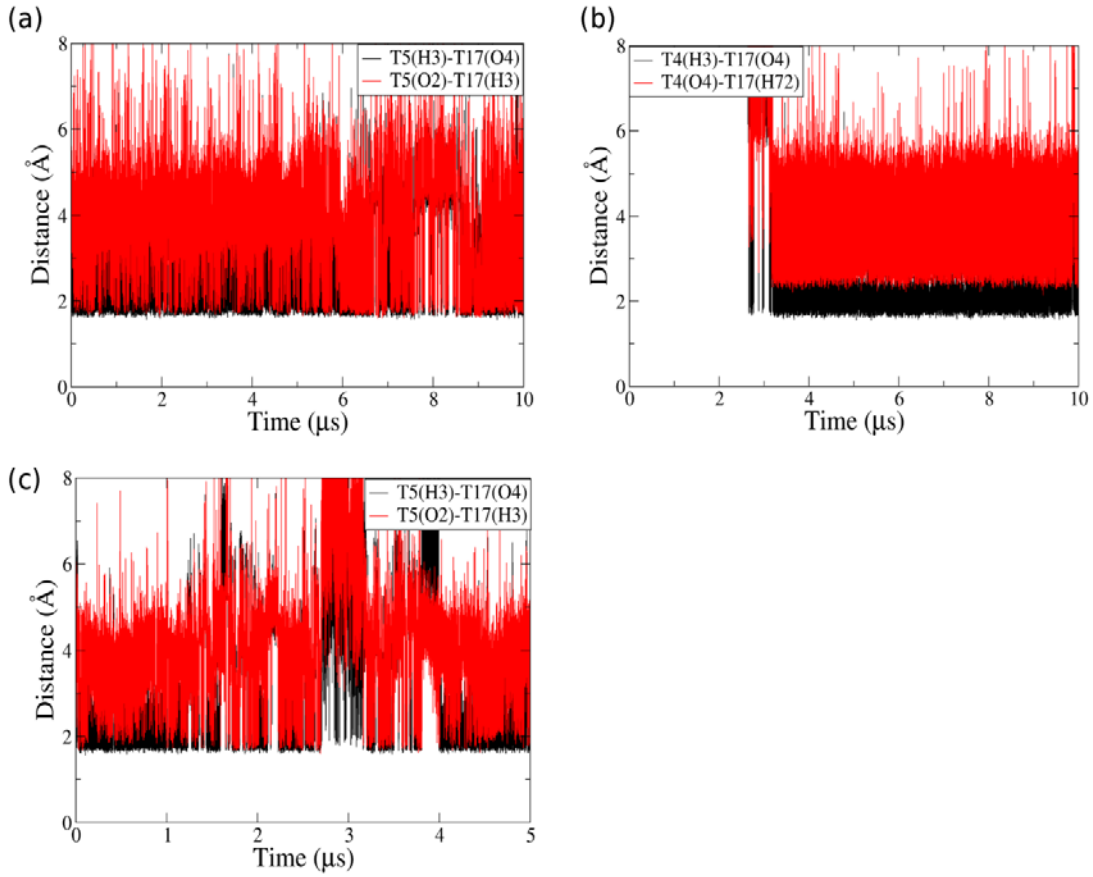

Figure S26: Distance plots of T5:T17 base pair sampled in 2KF8 in (a) bsc0χ_{OL4} and (c) OL15 simulations. (b) T4:T17 base pair was sampled in the bsc0$\chi_{OL4}\varepsilon\zeta_{OL1}$ simulation instead. In the panel (b), H72 refers to one methyl hydrogen of T17. Distance between T17(H72) and T4(O4) is shown as it is the closest hydrogen to T4(O4) for majority of the simulation time.

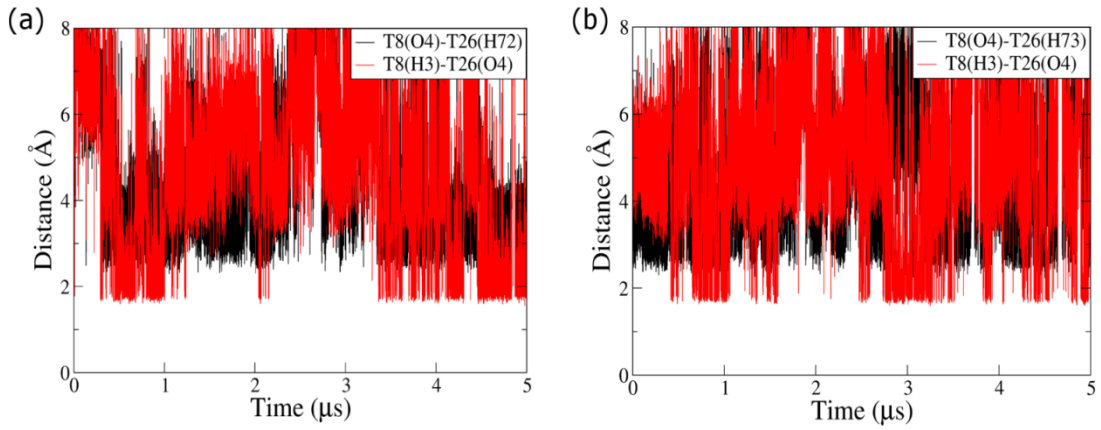

Figure S27: Distance plots of T8:T26 base pair sampled in the (a) K^+ and SPC/E and (b) K^+ and TIP3P simulations of 2MBJ in OL15 simulations. In the panels (a) and (b), H72 and H73 refer to the methyl hydrogens of T26. Distance T26(H72)-T8(O4) and T26(H73)-T8(O4) are shown in panels (a) and (b) as in majority of the frames, these are the closest hydrogens to T8(O4) in the respective simulations.

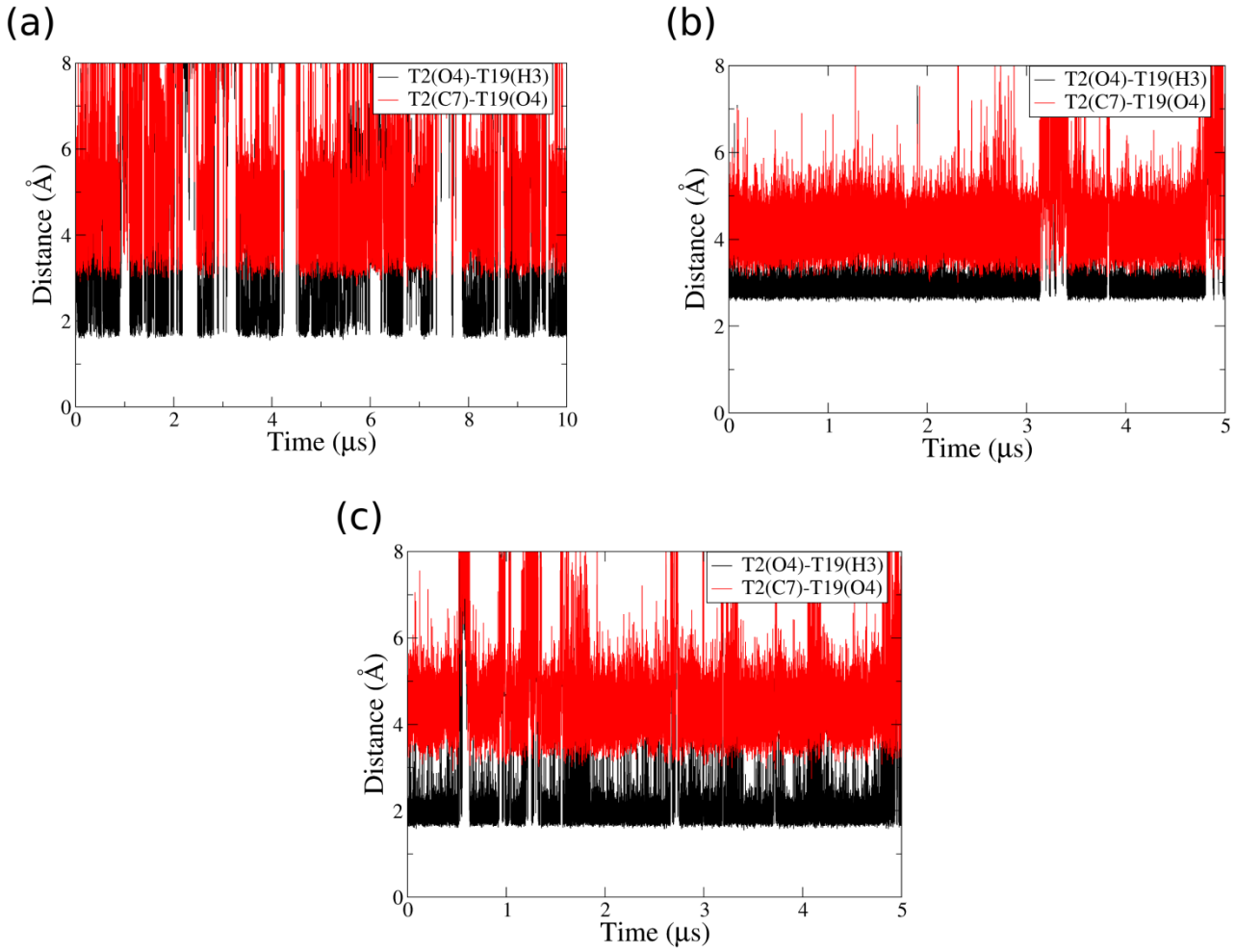

Figure S28: Distance plots of T2:T19 base pair in 2GKU (a) bsc0$\chi_{OL4}\varepsilon\zeta_{OL1}$, (b) K^+/SPC/E/OL15 and (c) K^+/TIP3P/OL15 simulations. T2 and T19 mainly interacted by a single hydrogen bond in all the three simulations.

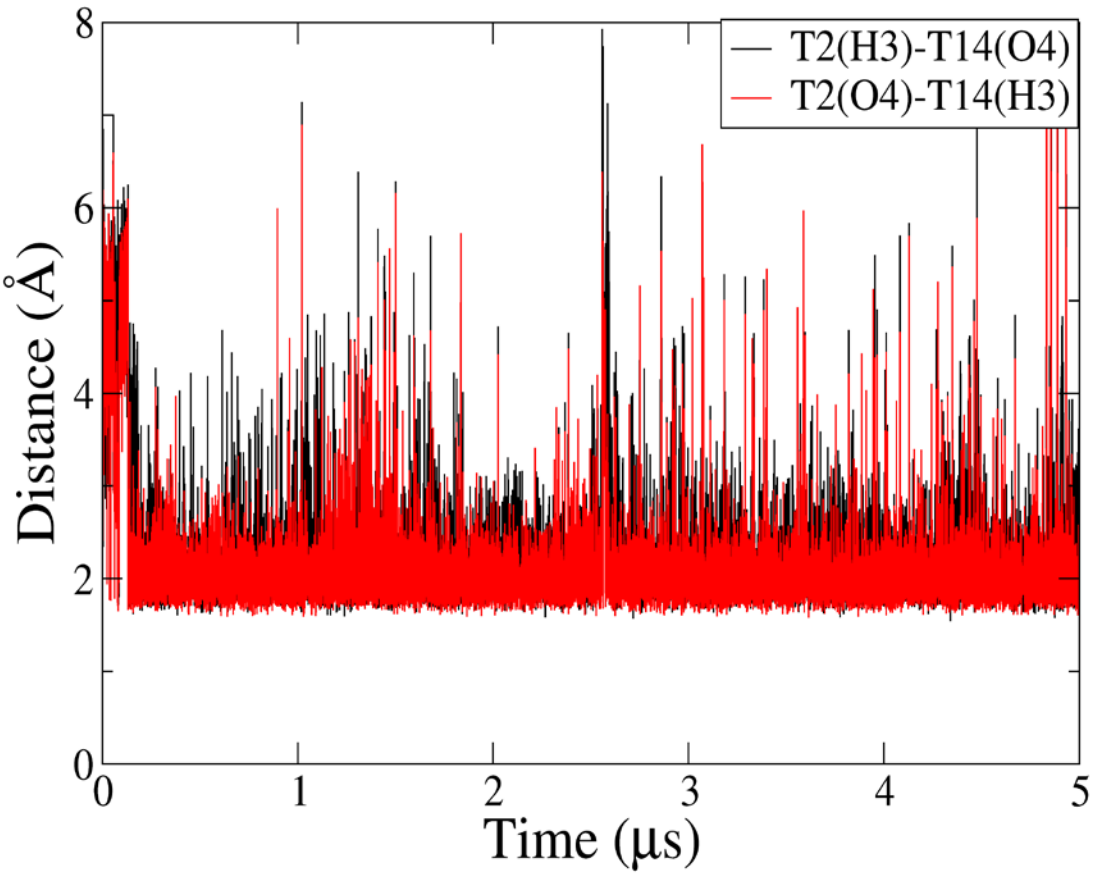

Figure S29: Distance plot of T2:T14 base pair sampled in the OL15 simulation of 2JPZ.

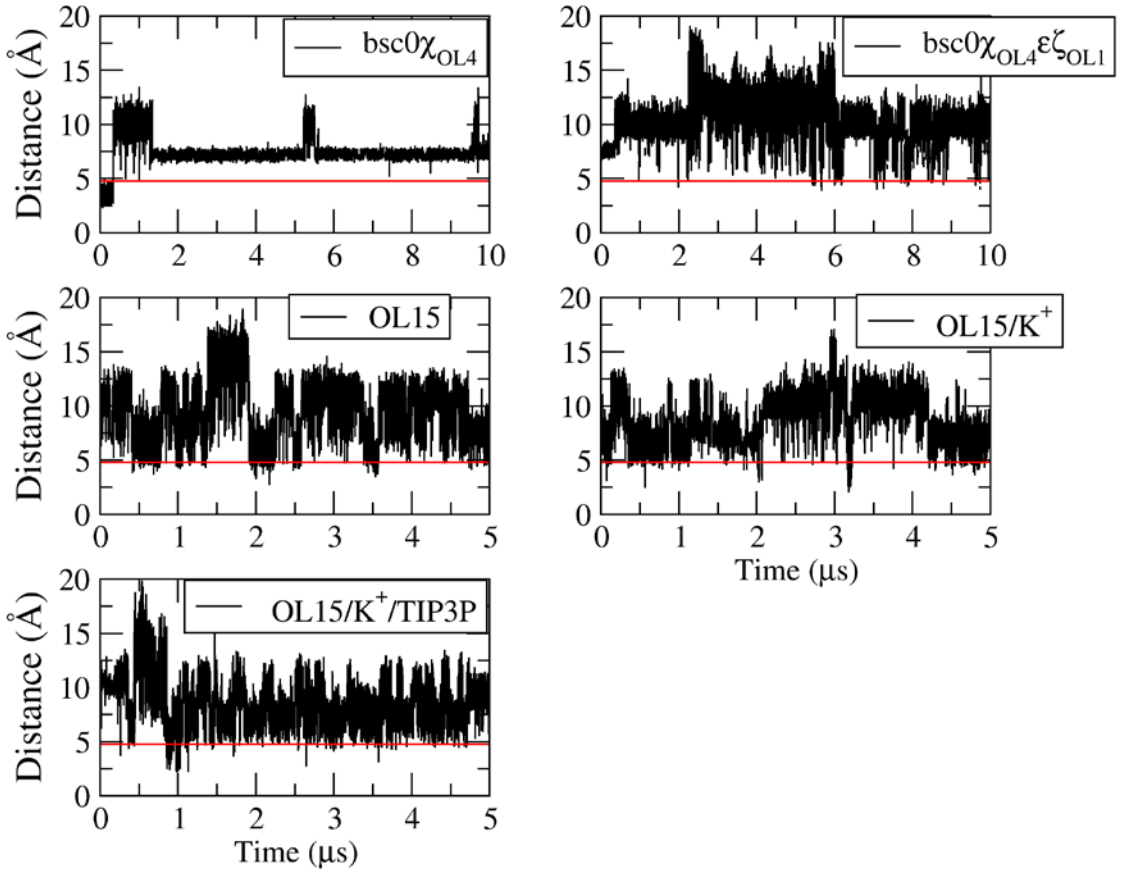

Figure S30: Distance plots of A3(H2) and A21(H2) proton pair in 2MBJ bsc0χ_{OL4}, bsc0$\chi_{OL4}\varepsilon\zeta_{OL1}$, OL15, OL15/$K^+$ and OL15/K^+/TIP3P simulations. Na^+ and SPC/E were the general choice and K^+ and TIP3P are explicitly mentioned in the figure when used in the simulation. The red line in each graph indicates experimental upper-bound distance between A3(H2) and A21(H2) protons.

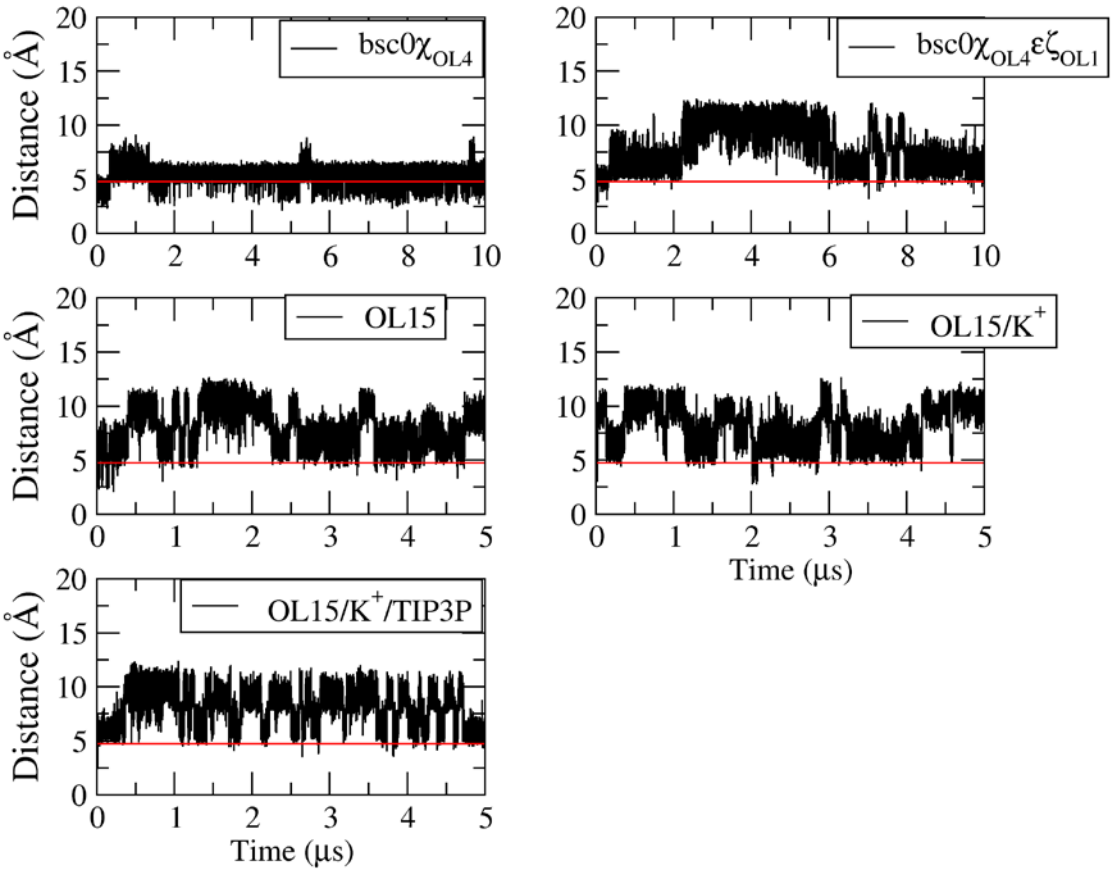

Figure S31: Distance plots of T20(H2′, H2″) and A21(H8) proton pair in 2MBJ bsc0χ_{OL4}, bsc0$\chi_{OL4}\varepsilon\zeta_{OL1}$, OL15, OL15/$K^+$ and OL15/K^+/TIP3P simulations. Na^+ and SPC/E were the general choice and K^+ and TIP3P are explicitly mentioned in the figure when used in the simulation. The red line in each graph indicates experimental upper-bound distance between T20(H2′, H2″) and A21(H8) protons.

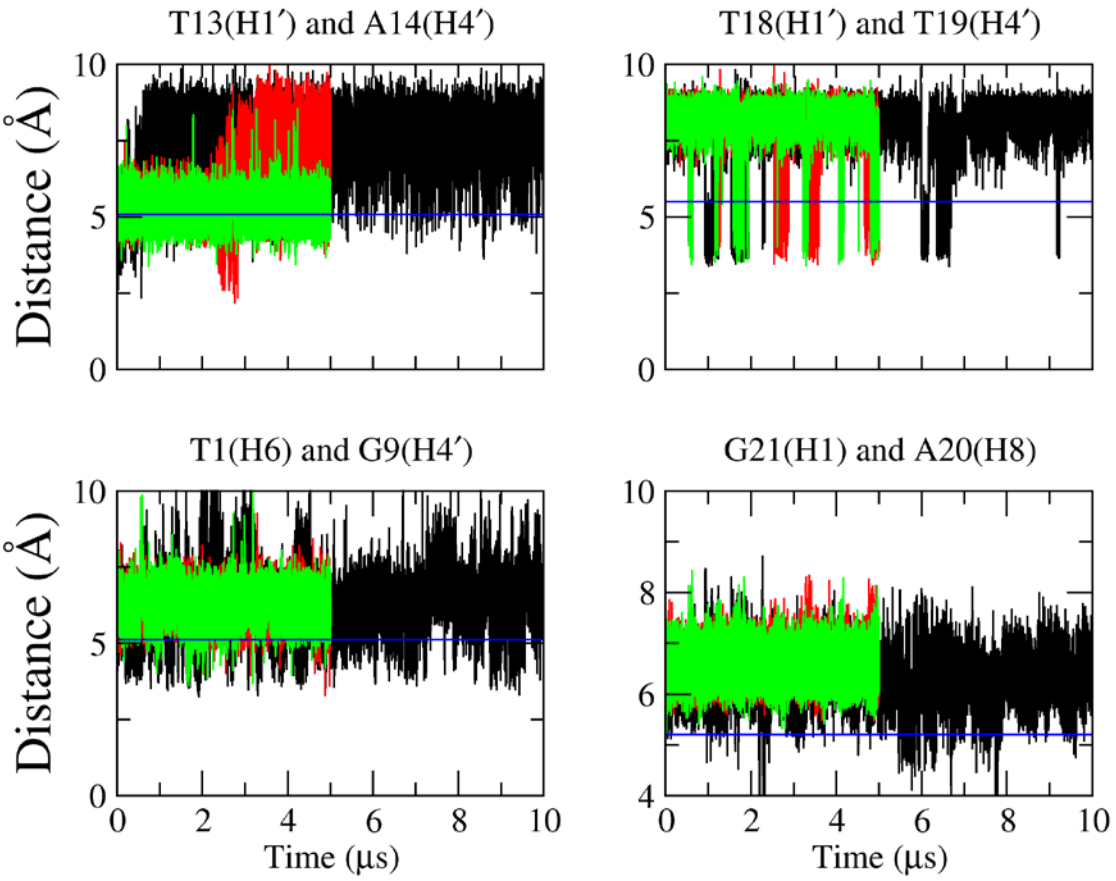

Figure S32: Distance plots of proton pairs that show major violations in 2GKU simulations. The proton pairs are mentioned as respective titles above the graphs. Distances in bsc0$\chi_{OL4}\varepsilon\zeta_{OL1}$, OL15/$K^+$ and OL15/K^+/TIP3P simulations are shown in black, red and green, respectively. The blue line in each graph indicates experimental upper-bound distance between the respective protons.

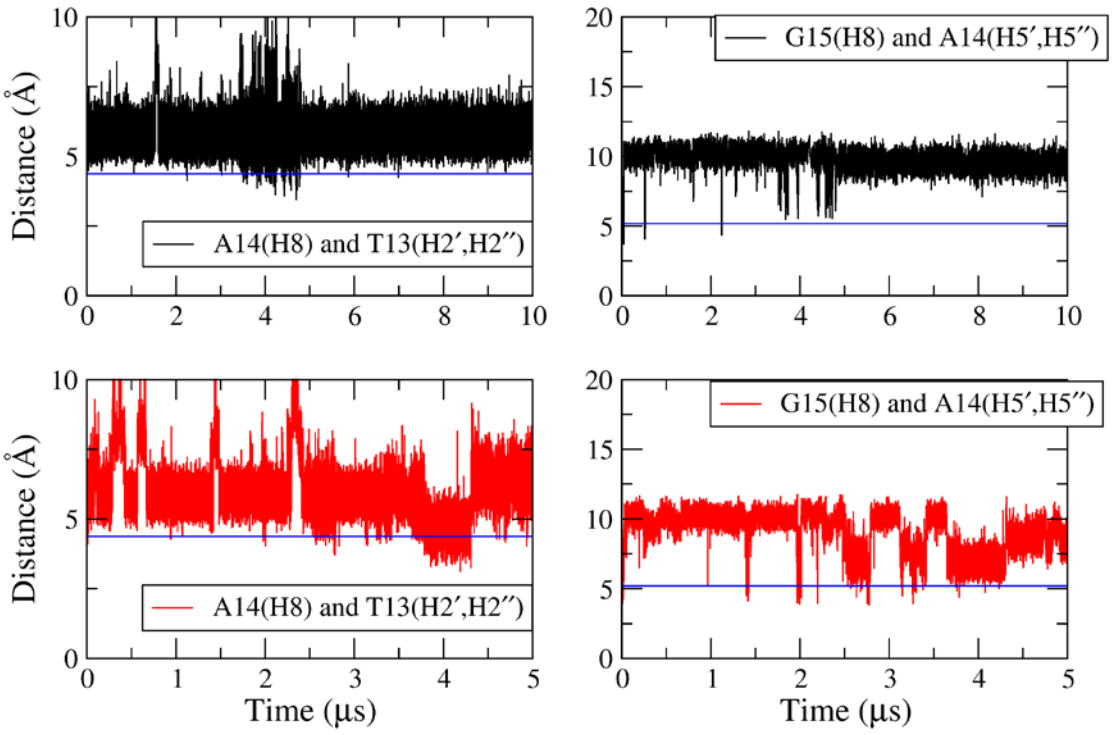

Figure S33: Distance plots of 2JSM [A14(H8) and T13(H2′, H2″)] and [G15(H8) and A14(H5′, H5″)] proton pairs in the bsc0$\chi_{OL4}\varepsilon\zeta_{OL1}$ and OL15 simulations. Distances in bsc0$\chi_{OL4}\varepsilon\zeta_{OL1}$ and OL15 simulations are shown in black and red, respectively. The blue line in each graph indicates experimental upper-bound distance between the respective protons.